JOURNAL OF GEOPHYSICAL RESEARCH, VOL. 102, NO. B5, PAGES 10,203–10,223, MAY 10, 1997

Segmentation and crustal structure of the western Mid-Atlantic Ridge flank, 25°25'-27°10'N and 0-29 m.y.

Brian E. Tucholke,[1] Jian Lin,[1] Martin C. Kleinrock,[2] Maurice A. Tivey,[1]
Thomas B. Reed,[3] John Goff,[4] and Gary E. Jaroslow[5,6]

Abstract. We conducted a detailed geological-geophysical survey of the west flank of the Mid-Atlantic Ridge between 25°25'N and 27°10'N and from the ridge axis out to 29 Ma crust, acquiring Hydrosweep multibeam bathymetry, HAWAII MR1 sidescan-sonar imagery, gravity, magnetics, and single-channel seismic reflection profiles. The survey covered all or part of nine spreading segments bounded by mostly nontransform, right-stepping discontinuities which are subparallel to flow lines but which migrated independently of one another. Some discontinuities alternated between small right- and left-stepping offsets or exhibited zero offset for up to 3-4 m.y. Despite these changes, the spreading segments have been long-lived and extend 20 m.y. or more across isochrons. A large shift (~9°) in relative plate motion about 24-22 Ma caused significant changes in segmentation pattern. The nature of this plate-boundary response, together with the persistence of segments through periods of zero offset at their bounding discontinuities, suggest that the position and longevity of segments are controlled primarily by the subaxial position of buoyant mantle diapirs or focused zones of rising melt. Within segments, there are distinct differences in seafloor depth, morphology, residual mantle Bouguer gravity anomaly, and apparent crustal thickness between inside-corner and outside-corner crust. This demands fundamentally asymmetric crustal accretion and extension across the ridge axis, which we attribute to low-angle, detachment faulting near segment ends. Cyclic variations in residual gravity over the cross-isochron run of segments also suggest crustal-thickness changes of at least 1-2 km every 2-3 m.y. These are interpreted to be caused by episodes of magmatic versus relatively amagmatic extension, controlled by retention and quasiperiodic release of melt from the upwelling mantle. Detachment faulting appears to be especially effective in exhuming lower crust to upper mantle at inside corners during relatively amagmatic episodes, creating crustal domes analogous to "turtleback" metamorphic core complexes that are formed by low-angle, detachment faulting in subaerial extensional environments.

Introduction

Over the past two decades, a large amount of geological and geophysical data has been collected at the axes of slow spreading ridges to examine how ocean crust is formed by the interplay of magmatic accretion and tectonic extension. However, to understand the full range of variation in processes of crustal formation, it is necessary to study off-axis crust. The off-axis record allows one to discriminate between dominant and subsidiary processes and to understand their spatial and temporal relations. It also provides information on flank-to-flank asymmetries in crustal accretion and tectonism, on plate-boundary changes caused by changes in relative plate motion, and on secondary aging effects in the ocean crust.

Detailed studies reaching a few million years off axis began in the mid-1980s [*Kuo and Forsyth*, 1988; *Sempéré et al.*, 1990; *Carbotte et al.*, 1991; *Grindlay et al.*, 1991], and three North Atlantic surveys (Figure 1) have collected grids of multibeam bathymetry and potential-field data as far as ~10 m.y. (~140 km) onto the flank of the Mid-Atlantic Ridge (MAR). In 1992 we conducted a detailed geological-geophysical survey out to 26-29 Ma crust on the west flank of the MAR between 25°25'N and 27°10'N, under the auspices of the Office of Naval Research Acoustic Reverberation Special Research Program (ARSRP) (Figure 1). This survey provides the longest detailed record of crustal structure currently available in any ocean basin. Because of programmatic goals the survey covered only one flank of the Mid-Atlantic Ridge, so the data do not address certain questions about cross-axis symmetries or completely document ridge development. Nonetheless, they provide significant new insights into the structure and origin of slow spreading crust. In the present paper we use these data to interpret MAR segmentation and to examine three issues: the factors that control ridge segmentation, the internal structure of spreading segments, and temporal variability in crustal accretion.

[1]Department of Geology and Geophysics, Woods Hole Oceanographic Institution, Woods Hole, Massachusetts.
[2]Department of Geology, Vanderbilt University, Nashville, Tennessee.
[3]Software Development Division, Oceanic Imaging Consultants, Honolulu, Hawaii.
[4]University of Texas Institute for Geophysics, Austin.
[5]MIT/WHOI Joint Program in Oceanography, Woods Hole Oceanographic Institution, Woods Hole, Massachusetts.
[6]Now at Sea Education Association, Woods Hole, Massachusetts.

Paper Number 96JB03896.
0148-0227/97/96JB-03896$09.00

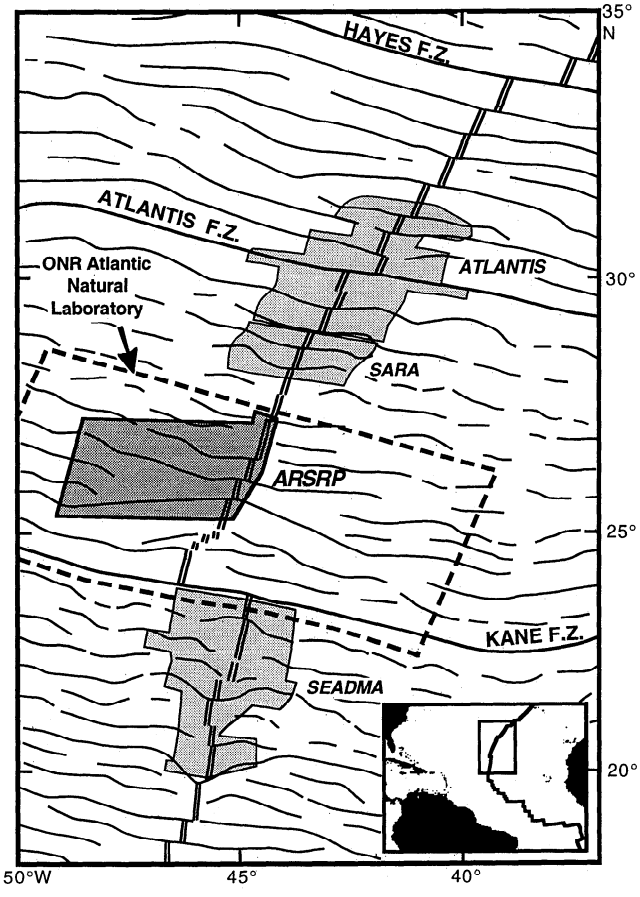

Figure 1. Location of the Acoustic Reverberation Special Research Program (ARSRP) study area over 0-29 Ma crust on the west flank of the Mid-Atlantic Ridge (MAR). The MAR axis (double line) and off-axis traces of transform faults (labeled) and NTDs (light lines) are interpreted from the marine gravity field derived from satellite altimetry [*Smith and Sandwell*, 1995]. Other detailed surveys extend ~10 m.y. off axis (Atlantis Fracture Zone (FZ) [*Sempéré et al.*, 1995; *Pariso et al.*, 1995], Segmentation Ancienne de la Ride Atlantique (SARA) [*Sloan and Patriat*, 1992; *Rommevaux et al.*, 1994], and SEADMA I [*Gente et al.*, 1995]).

Geological Background

Transform and nontransform discontinuites (NTDs) divide slow spreading crust into segments that extend along axis for an average of 50 ±30 km [*Macdonald*, 1986], and these discontinuities consistently create large-scale swell-and-trough topography in the ridge flanks (Figure 1). The fundamental cause of ridge segmentation appears to be the tendency of axial faulting, diking, and crustal accretion to orient orthogonal to the direction of relative plate motion and far-field stresses [*Menard and Atwater*, 1968; *Lachenbruch and Thompson*, 1972]. Consequently, mid-ocean ridges that are not oriented toward their pole of relative plate motion become segmented to accommodate this geometry. However, the factors that control the specific position, longevity, and length (along-isochron dimension) of individual spreading segments are unclear.

Two principal hypotheses have been proposed. The first, magmatic hypothesis ties the position of each spreading segment to the locus of an actively upwelling mantle diapir or focused zone of rising melt beneath the plate boundary [*Whitehead et al.*, 1984; *Crane*, 1985; *Kuo and Forsyth*, 1988; *Lin et al.*, 1990]. In this hypothesis, segment length can be inferred to relate to the magnitude of melt input into the segment [*Detrick et al.*, 1995]. Segments bounded by NTDs are observed to change length over time [e.g., *Sloan and Patriat*, 1992], and they may migrate along the plate boundary [*Müller and Roest*, 1992]; hence, according to the magmatic hypothesis, zones of asthenospheric upwelling do not produce constant volumes of melt through time, nor do they necessarily have stable positions beneath the plate boundary.

An alternate hypothesis suggests that there is mechanical control of segmentation caused by detachment faulting near segment ends, with intervening accommodation zones near segment centers [*Mutter and Karson*, 1992]. In this tectonic hypothesis, mantle upwelling and melt generation at the plate boundary are passive responses to variations in thermal state imposed by tectonic segmentation in the lithosphere, rather than deep-seated controls on the pattern of segmentation. This hypothesis implies that location, migration, and length change of segments bounded by NTDs are effectively random and that once a discontinuity disappears there is no reason for it to reappear in the same location along the plate boundary. The long record of segmentation history in our ridge-flank survey allows us to test these competing hypotheses, and we conclude that the magmatic hypothesis best explains the observed evolution of segments.

From near-axis studies, slow spreading ridge segments appear to exhibit significant internal structural variation [*Severinghaus and Macdonald*, 1988; *Tucholke and Lin*, 1994]. Segments can be divided into inside-corner (IC), segment-center (SC), and outside-corner (OC) tectonic setting along isochrons; each tectonic setting occupies roughly one third of segment length, although this varies with the magmatic and tectonic history of the segment. IC crust forms on the side of the spreading axis next to an active discontinuity and is characterized by anomalously shallow bathymetry, thinned crust and/or mantle exposures, irregular large-throw normal faults, and a paucity of volcanic morphologic features. OC crust is formed on the opposite side of the spreading axis next to the inactive trace of the discontinuity; it has more normal depth and crustal thickness, regular fault patterns, and more common volcanic features. These asymmetries are hypothesized to be caused by low-angle normal faulting (detachment faulting) near the ends of spreading segments [*Dick et al.*, 1981; *Karson*, 1990; *Tucholke and Lin*, 1994]. In this paper we examine the comparative structure of IC, SC, and OC crust in the long off-axis crustal record on the west flank of the MAR, and we find that observed spatial and temporal variations are consistent with the detachment-fault hypothesis.

Finally, we use the 29-m.y. crustal record in the ARSRP survey to investigate apparent cyclicity in crustal accretion. It has been suggested that cyclic magma input to the rift axis may occur on timescales as long as a few hundred thousand years, effectively the width scale of typical abyssal hills [*Pockalny et al.*, 1988; *Frey et al.*, 1993]. We find a prominent pattern of cyclic variation in residual mantle Bouguer gravity anomaly (and apparent crustal thickness) at significantly longer periods of ~2-3 m.y., and we interpret this variation to be caused by alternating episodes of magmatic versus relatively amagmatic extension.

Data Acquisition and Processing

The ARSRP survey extended approximately 200 km along seafloor isochrons by 400 km off axis on the west flank of the Mid-Atlantic Ridge (Figure 1). We acquired Hydrosweep multibeam bathymetry (Plate 1), which insonifies a seafloor swath up to twice water depth; HAWAII MR1 (HMR1) sidescan sonar and bathymetry, which covers a total swath width of 20 km; magnetics; gravity; and water gun and 3.5-kHz seismic reflection profiles. Tracks were oriented 20° to 30° from the direction of plate flow lines to obtain good sidescan-sonar backscatter from the dominant, ridge-parallel tectonic fabric, while still allowing us to acquire gravity and magnetic profiles subparallel to flow lines. Track line spacing was ~4 km over shallow seafloor near the ridge axis, and it increased regularly to 8-9 km over the deepest seafloor at the western edge of the survey. With this track spacing we acquired nearly total multibeam bathymetric coverage and 100-200% HMR1 coverage in each of two primary look directions (north and south). The line spacing was also close enough to allow reliable, three-dimensional (3-D) interpretation of gravity and magnetics in conjunction with mapped seafloor morphology.

Good GPS navigation was obtained for more than 23 hours each day, and dead reckoning based on Furuno speed and heading data was used to cover small GPS navigation gaps. The navigation data were smoothed to remove dithering of the GPS signal. Differential GPS data were also recorded on the ship and simultaneously at a base station at the Woods Hole Oceanographic Institution about 2000 km away. Comparison of these two GPS data sets and correlation with benchmarks ashore indicate that the smoothed GPS navigation is accurate to ~40 m and the differential GPS is accurate to ~20 m.

Hydrosweep bathymetry was processed using MB-System editing and processing software [*Caress and Chayes*, 1996]. Additional beam processing was conducted to reduce spurious cross-track roughness ("shingling") and seafloor "curl-up" in outer beams. The edited and corrected beam data were then combined with navigation to produce gridded bathymetry and contour maps (Plate 1). Bathymetric data were gridded at a 100-m interval, which is a reasonable average for conditions in this survey (ping repetition 15 s, ship speed 8-9 knots (4-4.5 ms^{-1}), and mean water depth 3500 m).

Total magnetic field was measured with a towed proton-precession magnetometer and was corrected for the regional field using the 1991 International Geomagnetic Reference Field [*International Association of Geomagnetism and Aeronomy (IAGA)*, 1987]. The data were merged with similarly corrected magnetics from the adjacent ridge-axis survey of *Purdy et al.* [1990], embedded within a larger Canadian compilation of magnetic data for the North Atlantic [*McNab et al.*, 1995] and then gridded using a minimum-curvature method with a nominal grid interval of ~1 km. All magnetic-anomaly

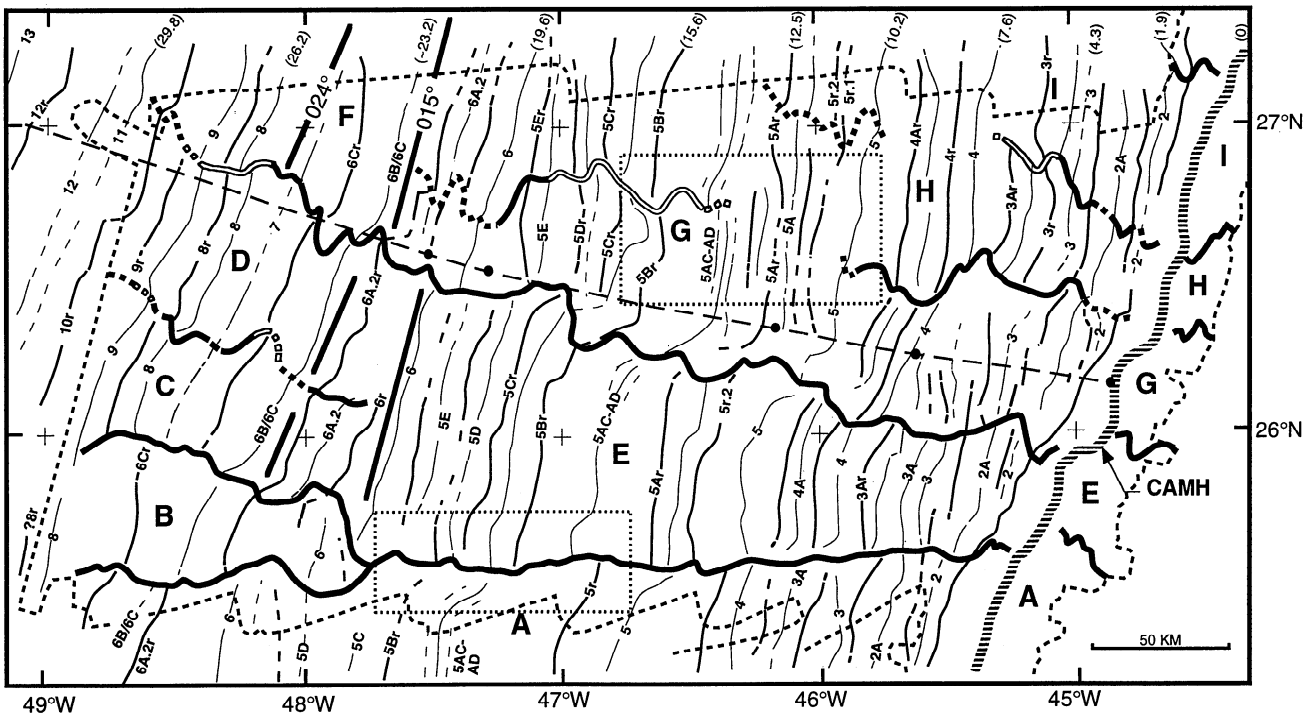

Figure 2. Magnetic anomalies and tectonic interpretation of segmentation in the ARSRP survey. Letters identify spreading segments discussed in text. Magnetic anomalies are numbered, and crustal ages in million years [*Cande and Kent*, 1992] are shown along the top of Figure 2 in parentheses; fine lines locate positive anomalies, and heavier lines locate negative (r) anomalies. Discontinuities, where identifiable in seafloor morphology, are shown as black heavy lines at right-stepping offsets, shown as open lines at left-stepping offsets, and shown as dashed where weakly developed. Note the major ~9° counterclockwise (CCW) change in orientation of magnetic anomalies following ~24 Ma (bold lines). Short dashes outline the limit of multibeam bathymetric coverage. Dotted boxes show locations of HAWAII MR1 (HMR1) sidescan-sonar images in Figures 5 and 6. The WNW trending dashed line is a synthetic flow line of relative plate motion based on *Collette and Roest* [1992].

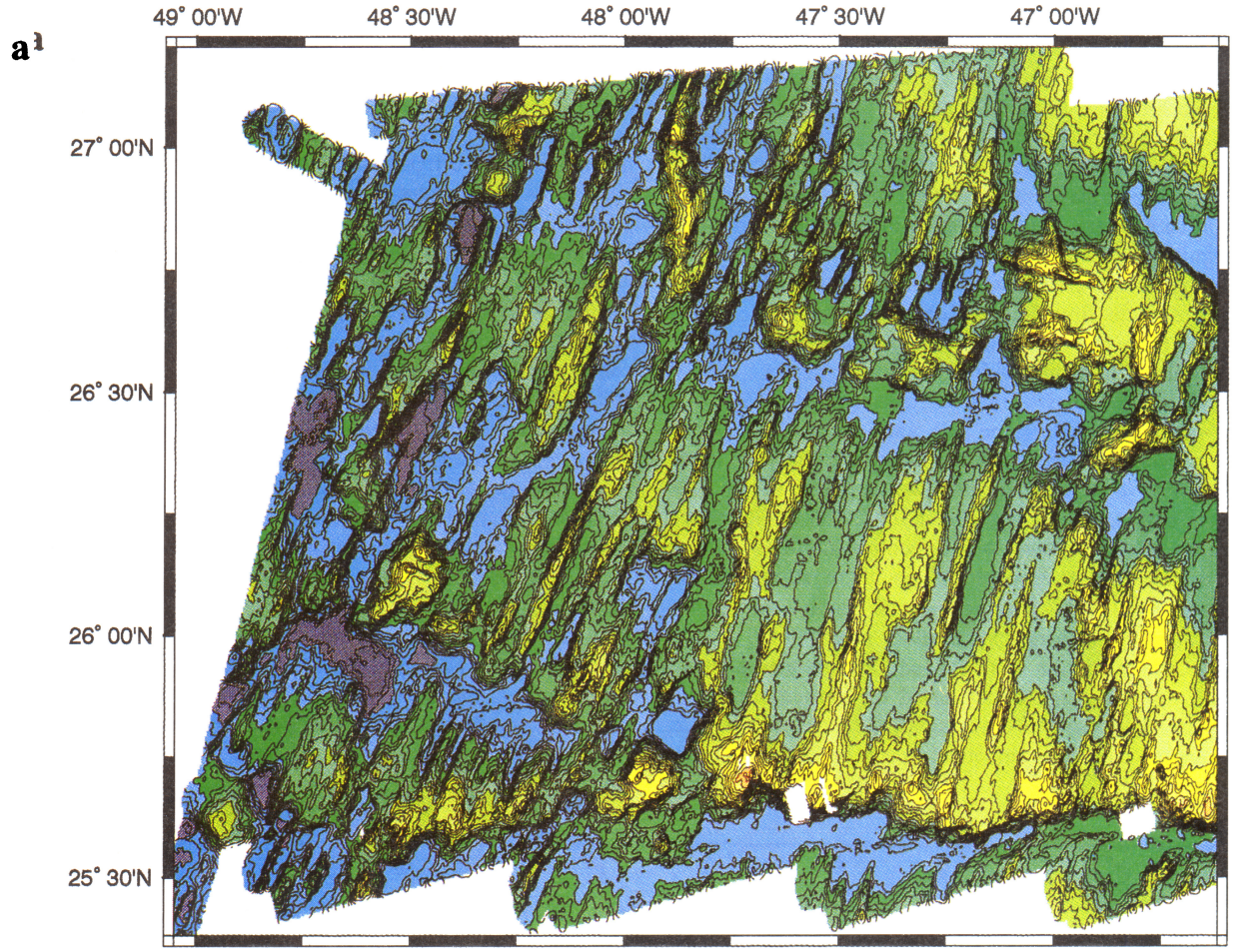

Plate 1. Bathymetry of the (a) western half and (b) eastern half of the ARSRP study area mapped with the Hydrosweep multibeam system. Contour interval is 100 m. In Plate 1b, Hydrosweep bathymetry is merged with SeaBeam bathymetry of *Purdy et al.* [1990] along the MAR axis at right.

data were reduced to the pole using a Fourier transform filtering approach [*Bhattacharyya*, 1965] to eliminate latitudinal skewness exhibited by the magnetic anomalies and to facilitate identification of anomalies for isochron-based studies (Figure 2). We also performed 3-D inversions for crustal magnetization, accounting for bathymetry and assuming a uniform-thickness magnetized layer [*Parker and Huestis*, 1974]. These inversions confirm the reduced-to-the-pole anomaly identifications. Detailed analysis of the crustal magnetization is given in a separate paper (M. Tivey and B. Tucholke, unpublished manuscript, 1997).

The gravity field was recorded on BGM-3 and KSS-30 gravimeters. Standard gravity data reduction was performed to obtain free-air anomalies, which exhibited rms crossover errors of only 1-2 mGal. To obtain mantle Bouguer anomalies, we used the Fourier transform technique of *Parker* [1973] to subtract the following crustal components from the free-air anomaly: (1) the attraction of the water/seafloor interface derived from multibeam bathymetry (we did not correct for sediment thickness, which is only a few tens of meters over most of the survey area and up to a few hundred meters in local ponds along discontinuities between segments) and (2) the attraction of the crust/mantle interface for a reference crust of uniform thickness (6 km) and density (seawater, crustal, and mantle densities of 1030, 2700, and 3300 kg m^{-3}, respectively, were assumed). To examine subseafloor density variations, the gravity data were further reduced to residual mantle Bouguer anomaly [*Kuo and Forsyth*, 1988; *Lin et al.*, 1990] by removing the effects of lithospheric cooling based on a 3-D passive-upwelling model [*Phipps Morgan and Forsyth*, 1988] (Figure 3). Relative crustal thicknesses were also calculated by downward continuation of the residual gravity anomaly to the base of a 6-km-thick crust with a crust/mantle density contrast of 600 kg m^{-3} [*Lin et al.*, 1990]. More detailed information on the gravity modeling is given by *Lin et al.* [1993] and J. Lin et al. (unpublished manuscript, 1997).

We towed the HMR1 sidescan-sonar/bathymetric mapping system [*Rognstad*, 1992] about 100 m below the sea surface to acquire backscatter imagery and phase-difference bathymetry at a ~50-m contour interval. The data were edited to remove bottom-detect and ping-flipping errors, processed (despeckled, destriped, angle-varying gain corrected, and backscatter was generated assuming a flat seafloor), merged with navigation, and digitally mosaicked.

Spreading Rates

The ARSRP survey extends from the MAR axis out to 26-29 Ma crust. Ages were determined by identifying all significant magnetic anomalies (Figure 2) from maps of crustal mag-

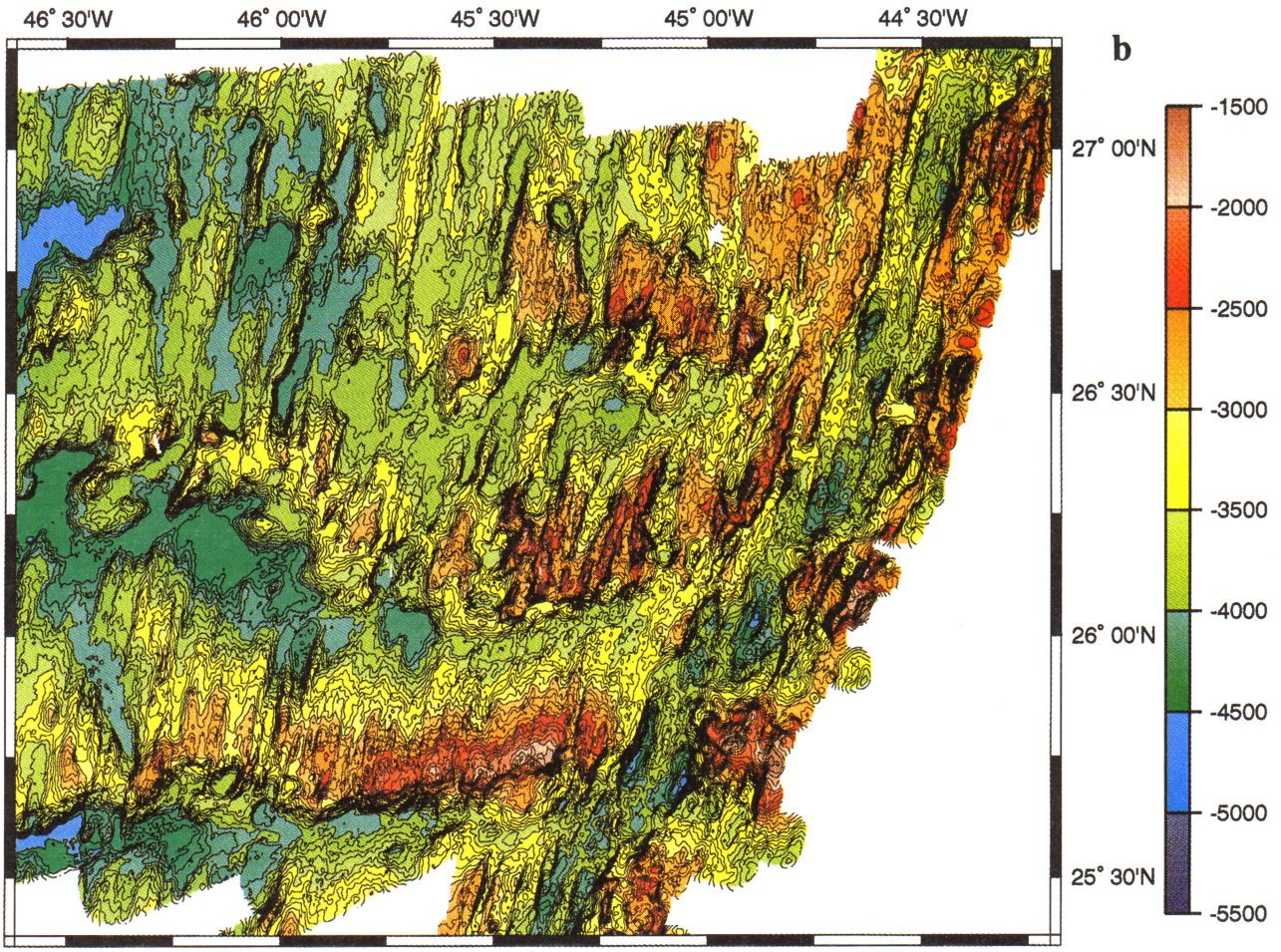

Plate 1. (continued)

netization. With minor exceptions, this part of the Mid-Atlantic Ridge flank exhibits a complete magnetic-anomaly record back to about anomaly 10R, which is observed in the northwest corner of the survey area (29 Ma on the *Cande and Kent* [1992] timescale used throughout this paper). In the southwest part of the survey, the oldest crust lies at anomaly 8 (~26.2 Ma).

Spreading half rates were calculated over the run (cross-isochron distance) of each spreading segment and then averaged within 5-m.y. bins to estimate overall spreading-rate variation on the ridge flank (Table 1). Average half rates range from 10 to 15 mm yr^{-1}, with the slowest spreading occurring over approximately the last 5 m.y. Within individual segments and over shorter time intervals, half rates range from ~8 to 23 mm yr^{-1}; these variations probably reflect short-lived episodes of asymmetric spreading or small ridge jumps.

Crustal Segmentation

Ridge-Axis Segmentation

Five significant, right-stepping nontransform discontinuities offset the MAR axis in the survey area (Figure 4), and they create spreading segments with characteristic structural patterns that are observed throughout the North Atlantic [*Phillips and Fleming*, 1977; *Rona and Gray*, 1980; *Sempéré et al.*, 1990]. In each segment, the rift valley is at least 3500-3700 m deep, and it is formed in large part by a pair of opposing, major inward facing normal fault zones (bold lines, Figure 4). Each rift valley also contains an axial ridge that averages 200-500 m high and 2-4 km wide, and exhibits numerous volcanic cones [*Smith and Cann*, 1990]. The positions of the axial ridges correlate with the central anomaly magnetization high, which is thought to mark the neovolcanic zone of most recent crustal accretion [*Klitgord*, 1976].

The nontransform discontinuities contain basins that define the deepest points along the MAR rift valley. The neovolcanic ridges terminate in the discontinuities either by merging into the old side margins of these terminal basins (e.g., 26°N, Figure 4) or by entering and bisecting the basins (e.g., 25°40'N). These relations are very similar to those observed in larger, transform discontinuities where the neovolcanic ridge skirts or bisects the nodal basin at ridge-transform intersections [*Karson and Dick*, 1983; *Dick et al.*, 1991]. Unlike transform offsets, however, the NTDs show no evidence of ridge-normal strike-slip faults linking the tips of the offset neovolcanic zones.

Within our study area, the southern two NTDs have the largest offsets, about 15 km. In these offsets the ends of the neovolcanic zones do not overlap, and they are girdled by deep (4200 m) terminal basins and separated from one another by a large ridge or septum that is subparallel to the adjacent rift valleys (Figure 4). The northern three discontinuities have smaller offsets of 6-10 km, they have no large septa, and the associated terminal basins are smaller and shallower. A small

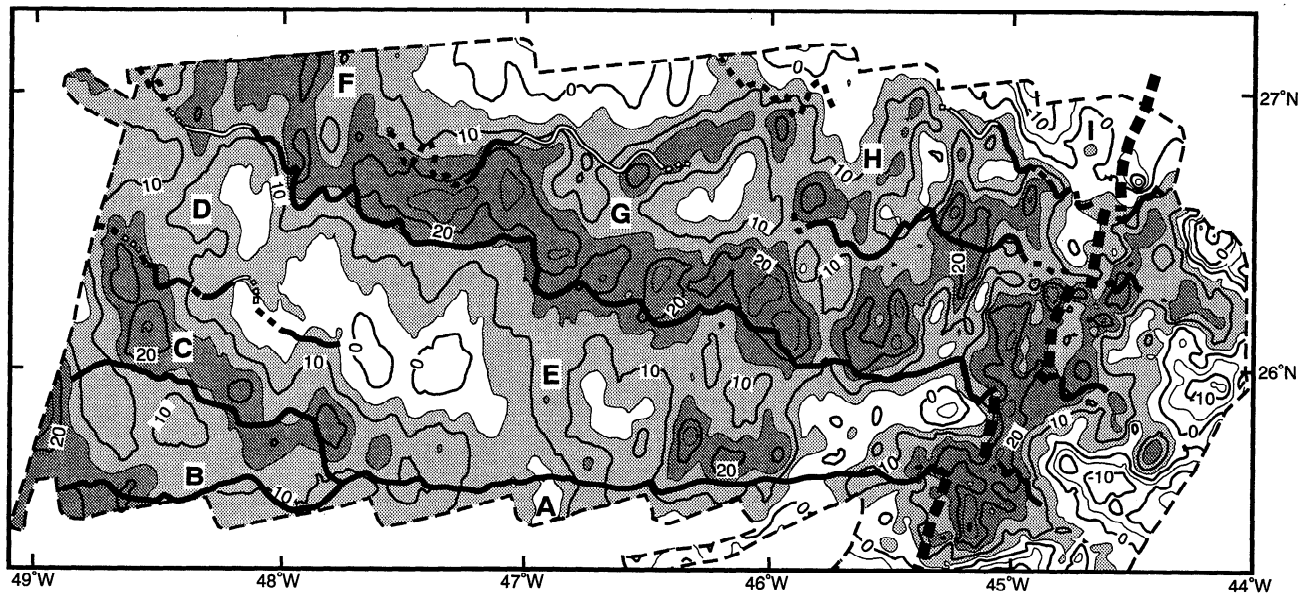

Figure 3. Residual mantle Bouguer anomaly (in milligals) for the ARSRP survey, derived as described in text. Segment boundaries and letter identifications are as in Figure 2. Note the cross-isochron bands of gravity lows at segment centers and gravity highs over inside-corner (IC) crust and the alternating relative highs and lows at ~2-3 m.y. intervals within these bands. From the MAR axis eastward, the residual mantle Bouguer anomaly was calculated from gravity data of *Rona and Gray* [1980].

amount of neovolcanic-zone overlap (3-4 km) occurs at two of these NTDs (26°18'N and 26°35'N). The differing robustness of larger- and smaller-offset discontinuities along the MAR axis is also observed in ridge-flank traces of NTDs, as discussed below.

Ridge-Flank Discontinuities

From combined analysis of crustal morphology, magnetics, and gravity anomalies, we identified discontinuities that divide the ridge flank into nine spreading segments (A-I in Figures 2-4). Observed paleooffsets across the discontinuities vary from 0 to 58 km in distance and 0 to 3 m.y. in age (Figure 2). Most offsets were less than ~30 km and therefore are considered to be nontransform discontinuities. Right-stepping offsets predominate, with three notable exceptions. The D-F discontinuity was a small left-stepping offset from anomaly 9 to younger than anomaly 8 (~27.5 to 25.6 Ma), and it rapidly changed its sense of offset immediately before and after this time (Figure 2). More significantly, the G-H offset was left-stepping between anomalies ~5E and 5AC (~18.6 to 13.9 Ma). For nearly 4 m.y. after this time (to anomaly 5, ~ 10.2 Ma) the discontinuity had zero offset; in this interval there is no disruption of crustal structure to suggest the presence of a discontinuity (Plate 1 and Figure 5), and a prominent residual gravity low is observed (Figure 3). Following 10.2 Ma, the discontinuity is again identifiable as a right-stepping feature. Finally, the H-I discontinuity had a very small offset (<10 km) for most of its history, and small right- and left-stepping forms have occurred intermittently (Figure 2). From anomaly 5 to near anomaly 3Ar (~10.2 to 7 Ma) this discontinuity had zero offset, lacked any notable structural disruption at the seafloor, and was crossed by both a residual gravity high and a low (Figure 3).

Discontinuities between spreading segments usually appear as geomorphic troughs crossing the ridge flank (Plate 1), and their axes of maximum depth (AMD) correlate well with magnetic-anomaly offsets (Figure 2). The discontinuities exhibit overall orientations subparallel to flow lines of relative plate motion (Figure 2), but they have migrated independently of one another. In detail, the discontinuities have irregular traces that meander with wavelengths and amplitudes of a few kilometers up to about 10 km. Isochron-parallel abyssal hills within the adjacent spreading segments sometimes interdigitate across the discontinuities (Plate 1), suggesting intermittent, competing expansion and contraction of the segments much like dueling propagating rifts [*Macdonald et al.*, 1988]. Like their modern expressions at the MAR axis, the NTDs rarely exhibit internal structure indicating ridge-normal, strike-slip deformation.

The discontinuity between segment A and segments B and E (Figure 2) differs significantly from the other NTDs. It does not follow plate flow lines but has migrated northward along the plate boundary at an average rate of 2 km m.y.$^{-1}$ over the past 26 m.y. During part of its history, ~17 to 11 m.y. ago (anomalies 5D to 5r), the A-E discontinuity reached an offset of 35 to 58 km (2-3 m.y.), placing it within the lower range of offsets usually associated with transform faults. Here the dis-

Table 1. Average Spreading Half Rates for West Flank of Mid-Atlantic Ridge

Anomaly	Age, m.y.	Rate, mm yr^{-1}
0 - 3r	0 - 5.3	10
3r - 5	5.3 - 10.2	13
5 - 5Br	10.2 - 15.6	15
5Br - 6	15.6 - 19.6	15
6 - 7	19.6 - 25.0	13
7 - 11	25.0 - 29.8	15

continuity exhibits two features characteristic of transform offsets. First, several traces of probable strike-slip faults are observed, oriented roughly orthogonal to the ridge axis (Figure 6). Second, the trend of the discontinuity (primarily in the western section) deviates from the overall pattern of northward migration and is nearly parallel to plate flow lines (Figure 2). The A-E offset subsequently decreased to about 30 km (~2 m.y.) from 11 Ma to 5 Ma (to anomaly 3), and after 5 Ma it ranged between 10 and 20 km. With these reduced offsets the discontinuity again behaved like an NTD and migrated very steadily northward to its current ridge-axis position at 25°40'N. From these observations, the critical transition from transform to nontransform behavior occurs at an age offset of ~2 m.y. (~30-35 km at observed spreading rates). At this offset, the truncating lithosphere at the ridge axis on the old side of the discontinuity should be about 13 km thick, based on a standard cooling model [*Parker and Oldenburg*, 1973]. During the period 17 to 11 Ma when the A-E discontinuity exhibited limited transform characteristics, the truncating lithosphere nominally would have been up to 15 km thick.

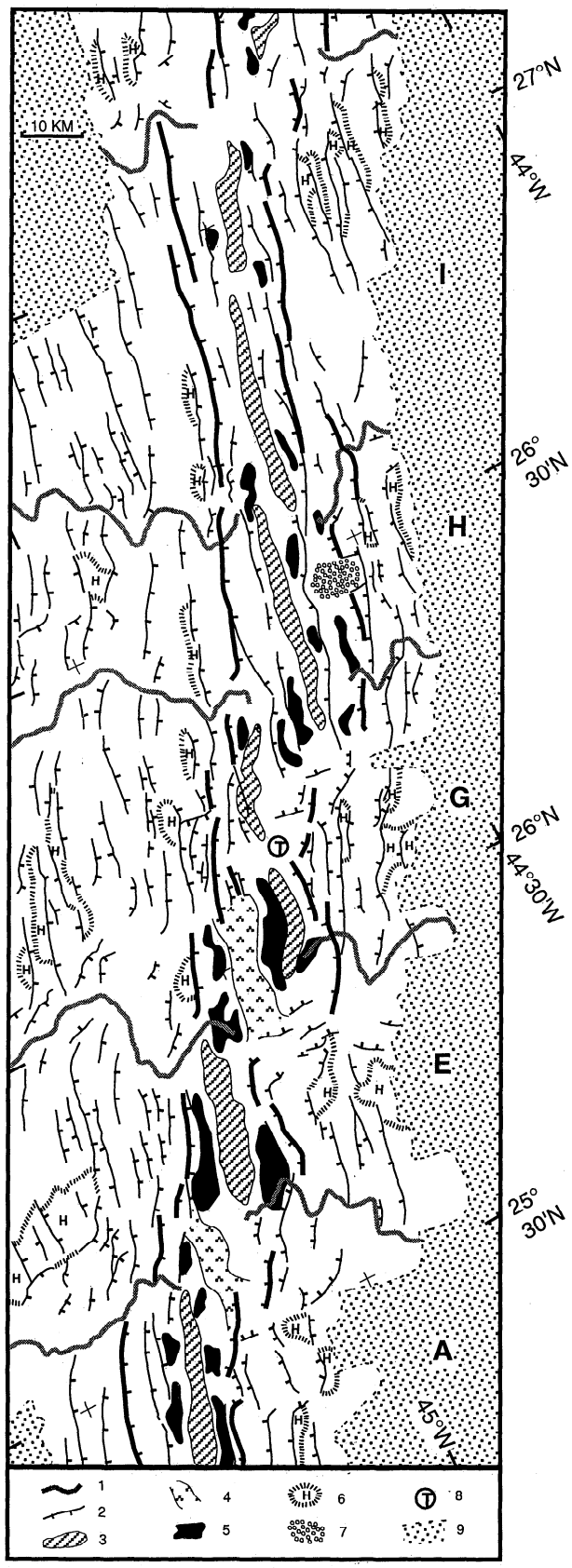

Basement depths along the axes of the discontinuities and on adjacent IC and OC crust all roughly follow a square-root-of-age relation, although they are offset from a standard curve (Figure 7). Compared to normal crust, IC crust consistently is elevated and OC crust is depressed; IC depths average about 600-700 m shallower than similar age OC crust on the opposite side of the discontinuity. Segment centers, or IC and OC depths averaged together, would approximately follow the age-depth curve illustrated in Figure 7. Depths along the AMDs of the discontinuities run about 700 m deeper than depths of normal crust outside the discontinuities, and they are about 1000-1200 m deeper than adjacent IC crust (Figures 7a and 7c). Uplift of rift-valley crust to form the rift mountains is clearly observed at 0-3 Ma; OC crust and crust within discontinuities is typically uplifted by 500 m, and IC crust is uplifted by as much as 1000 m (Figure 7).

Axial depths of discontinuities are affected by the magnitude of age offset (Figure 8a). At 0 to 1.5 m.y. offset, depths increase significantly with offset, but at larger offsets, depths are more constant and average ~1000 m. Most of the increase in depth with offset can be ascribed to increased differential between discontinuity depth and IC depth (Figure 8b), and there is only a small differential between discontinuity depth and OC depth (Figure 8c). Overall, the elevation of IC crust above coeval OC crust on the opposite side of a discontinuity steadily increases with increasing age offset in the 0- to 3-m.y. offset range (Figure 8d).

Segment Evolution

Of the nine crustal segments identified on the MAR flank, at least four were very long lived (Figure 2). Segment A origi-

Figure 4. Structural interpretation of the MAR axis at the eastern edge of the ARSRP area. Letter identifications of segments are as in Figure 2. Explanations are as follows: 1, nontransform discontinuities (NTDs); 2, normal faults, major faults primarily defining the rift valley are emphasized by heavy lines; 3, neovolcanic zones, defined by elevated volcanic ridges and cones [*Smith and Cann*, 1990] and by location of central anomaly magnetization high; 4, prominent septa crossing discontinuities between segments; 5, significant basins in axial valley and NTDs; 6, major bathymetric highs in bordering rift mountains; 7, massive rockslide in rift-valley wall [*Tucholke*, 1992]; 8, TAG hydrothermal mounds [*Rona et al.*, 1986]; and 9, limit of multibeam bathymetric coverage.

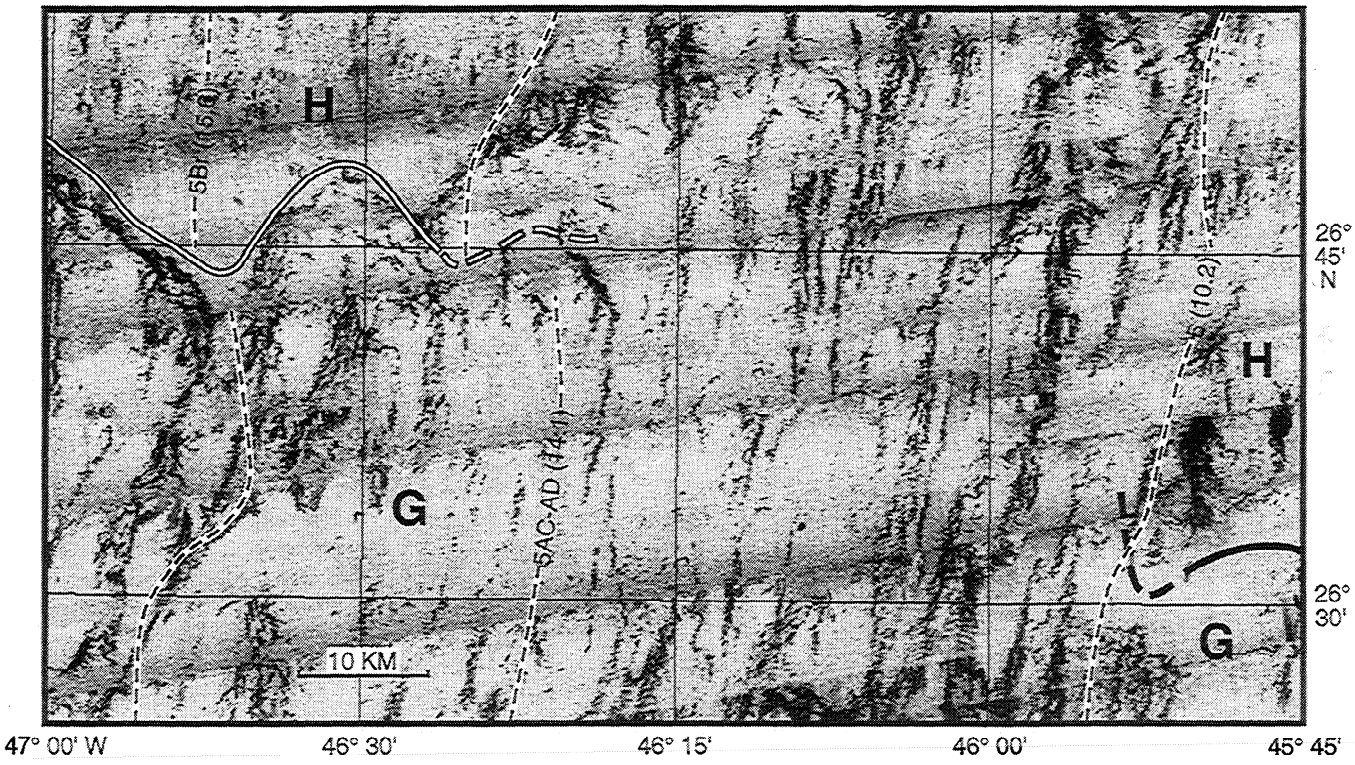

Figure 5. HMR1 sidescan-sonar mosaic (insonification toward south) showing crustal structure of a portion of the G-H nontransform discontinuity (location in Figure 2). Selected magnetic anomalies (dashed) are identified, with ages in million years. At center, there is no offset in magnetic anomalies between segments G and H, and through-going faults show no structural manifestation of the discontinuity. In contrast, there are significant structural disruptions at the discontinuity outside the zero-offset region.

nated prior to 26 Ma, and three other segments (E, G, and H) formed about 22-20 Ma, the first by consolidation of preexisting segments C and D and the latter two by division of segment F. Segment lengths have averaged about 50 km over the past 29 m.y., similar to the average spacing between transform and nontransform discontinuities observed at the present ridge axis. However, segment E attained an initial length of ~100 km following the consolidation of segments C and D, and it has shrunk steadily to a present length of about 40 km. Segment F also was at least 80 km long at 22 Ma prior to its division into segments G and H.

A distinct counterclockwise (CCW) change in relative plate motion occurred about 24-22 Ma (Figure 2). Before this time, orientation of abyssal hills, faults, and magnetic anomalies averaged about 024°, and subsequent orientations were about 015°, a change of ~9°. This reorientation coincides with the timing of a CCW shift in relative plate motion observed in structure of the Kane Fracture Zone (FZ) to the south [*Tucholke and Schouten*, 1988]. The disappearance of segments C and D and the initiation of segments G and H at about this time suggest that the plate-motion change strongly affected plate-boundary structure. The effect, however, seems not to have been synchronous along the rift axis. North of the D-F discontinuity, magnetic anomalies and structural lineations show CCW reorientation at ~24-23 Ma, with new segments G and H forming by 22 Ma (Figure 2). South of the discontinuity the reorientation appears to have occurred ~22-20 Ma, and segments C and D merged toward the end of this period. Farther south, segment B failed within 1-2 m.y. after the disappearance of the C-D discontinuity.

Following 20 Ma, frequent changes in spreading direction are suggested by diverse orientations of structural lineations and magnetic anomalies (Plate 1 and Figure 2). *Sloan and Patriat* [1992] derived a record of frequent relative plate-motion changes of up to 11° within the latter half of this period, based on the Segmentation Ancienne de la Ride Atlantique (SARA) survey out to 10 Ma crust (Figure 1). The observed morphology and magnetic isochrons in our study area are irregular enough that no clear correlation can be made with the *Sloan and Patriat* [1992] plate-motion history, and we currently lack data on the conjugate east flank of the MAR with which to make detailed plate reconstructions. However, the observed segments have maintained a relatively stable geometry over the past 20 m.y., and the frequent plate-motion changes therefore appear not to have had a significant effect on the pattern of plate-boundary segmentation.

Internal Structure of Segments

Variations Over Segment Length

A prominent feature of individual ridge segments is their along-isochron asymmetry in depth. Right-stepping offsets occur at most discontinuities, so most segments have elevated IC crust along their southern margins and the seafloor slopes northward toward deeper OC crust (Plate 1). This characteristic is best developed within segment E, particularly in crust younger than 10 Ma, and it is least developed where the NTD offsets are very small (e.g., segments H and I, Plate 1 and Figure 7d). It is noteworthy that excess IC elevation develops

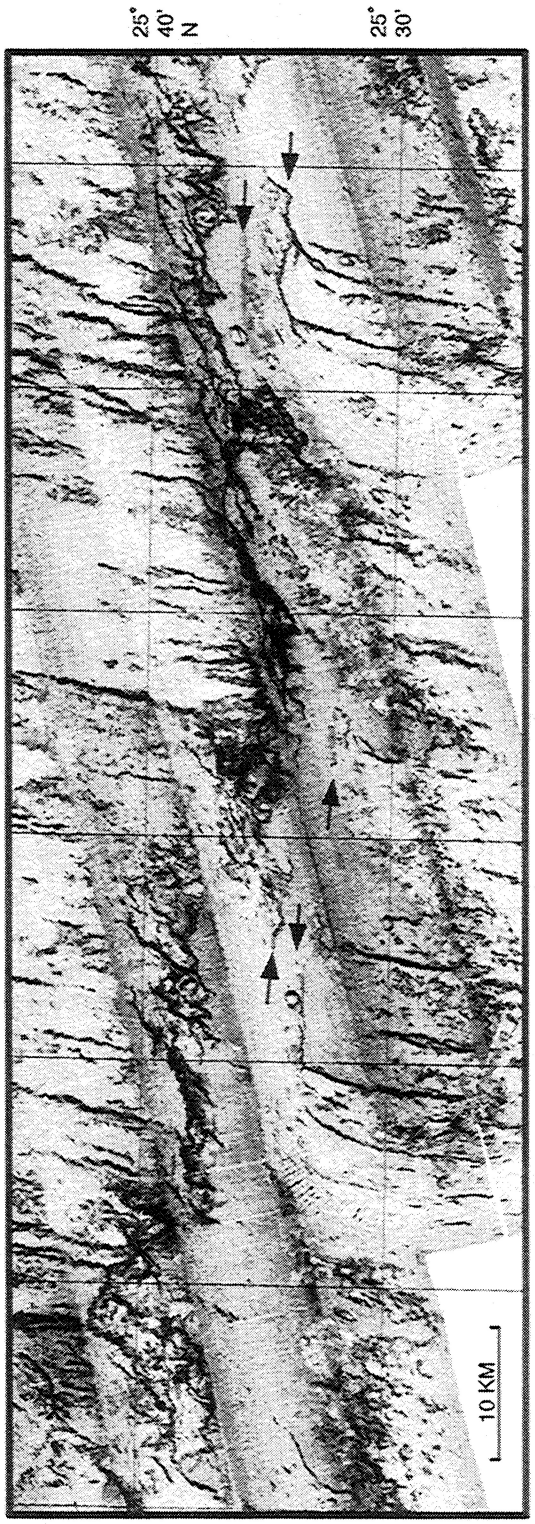

Figure 6. HMR1 sidescan-sonar mosaic (insonification toward north) showing crustal structure of the segment A-E discontinuity when it was a small (~35-58 km) transform offset at ~18-11 Ma. Location shown in Figure 2. Arrows locate probable strike-slip faults orthogonal to the MAR axis; much basement structure is masked by sediment (smooth areas) deep within the discontinuity. Irregular faults that typify IC crust north of the discontinuity crust are mostly within ~10 km of the segment edge; at the upper left (47°40'-47°50'W), a large IC dome (see Plate 1) exhibits highly irregular faults and possible slump scars. Outside-corner (OC) crust south of the discontinuity shows linear faults curving toward the MAR axis, as well as frequent small volcanic mounds and cones.

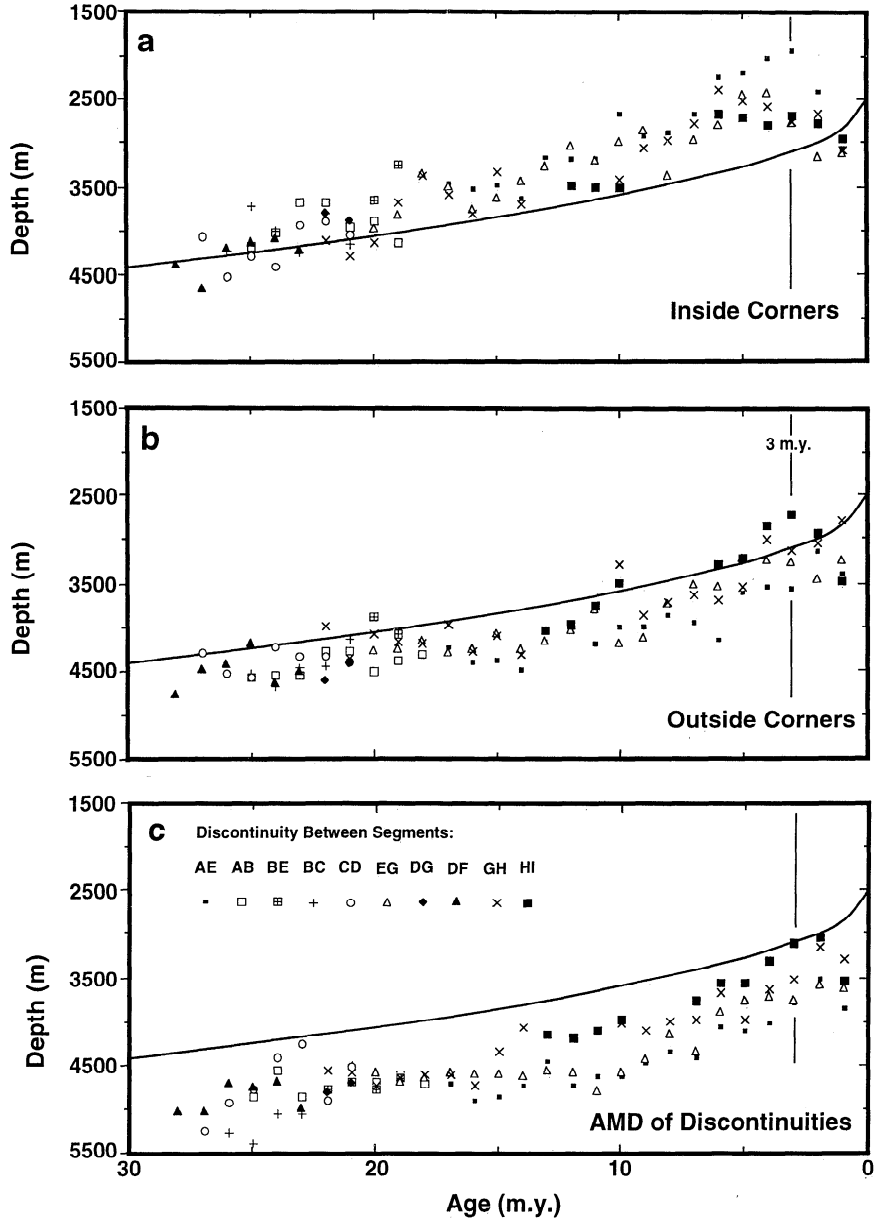

Figure 7. Age-depth relations for ocean crust (sediment cover removed) at segment (a) ICs, (b) OCs, and (c) along axes of maximum depth (AMD) of the adjacent discontinuities. A typical age-depth curve ($D = 2500$ m + $350t^{1/2}$ [*Parsons and Sclater*, 1977]) is repeated in each panel for reference. IC depths were picked every 2 km along the segment run, following the axis of IC minimum depth; this axis usually lies 10-20 km from the AMD of the adjacent discontinuity. Depths were then averaged in 1-m.y. bins and plotted. The same picking and binning intervals were used for OC and AMD depths. OC depths were picked along a profile offset 12 km along isochrons from the AMD of the adjacent discontinuity. Note that the MAR axial valley reaches to ~3 m.y. off axis in all profiles.

even when a segment has two inside corners. An example occurs in segment G, which had a right-stepping offset at its southern discontinuity and a left-stepping offset at its northern discontinuity from ~18.6 to 13.9 Ma (anomalies 5E to 5AC, Figure 2 and ~46°20'W to 47°05'W, Plate 1). Both inside corners here have markedly elevated topography, and they are separated by a depressed saddle at the segment center.

Character of faulting also varies markedly over the length of a segment. At segment centers most normal faults and associated abyssal hills are linear, have moderate to low amplitude, and are approximately orthogonal to plate flow lines (Plate 1). These structural elements usually continue uninterrupted into OC crust; within 10-15 km of a discontinuity, OC crust often exhibits faults that curve toward the ridge axis, and the associated curved abyssal hills plunge gently into the discontinuity. Similar curvature has been observed at both NTDs and transform offsets elsewhere in the Atlantic [*Tucholke and Schouten*, 1988; *Sempéré et al.*, 1995] and in the Pacific [e.g., *Searle*, 1983], and it is thought to result from rotation in the direction of least principal compressive stress near the ridge-discontinuity intersection.

Faults and abyssal hills at segment centers also continue

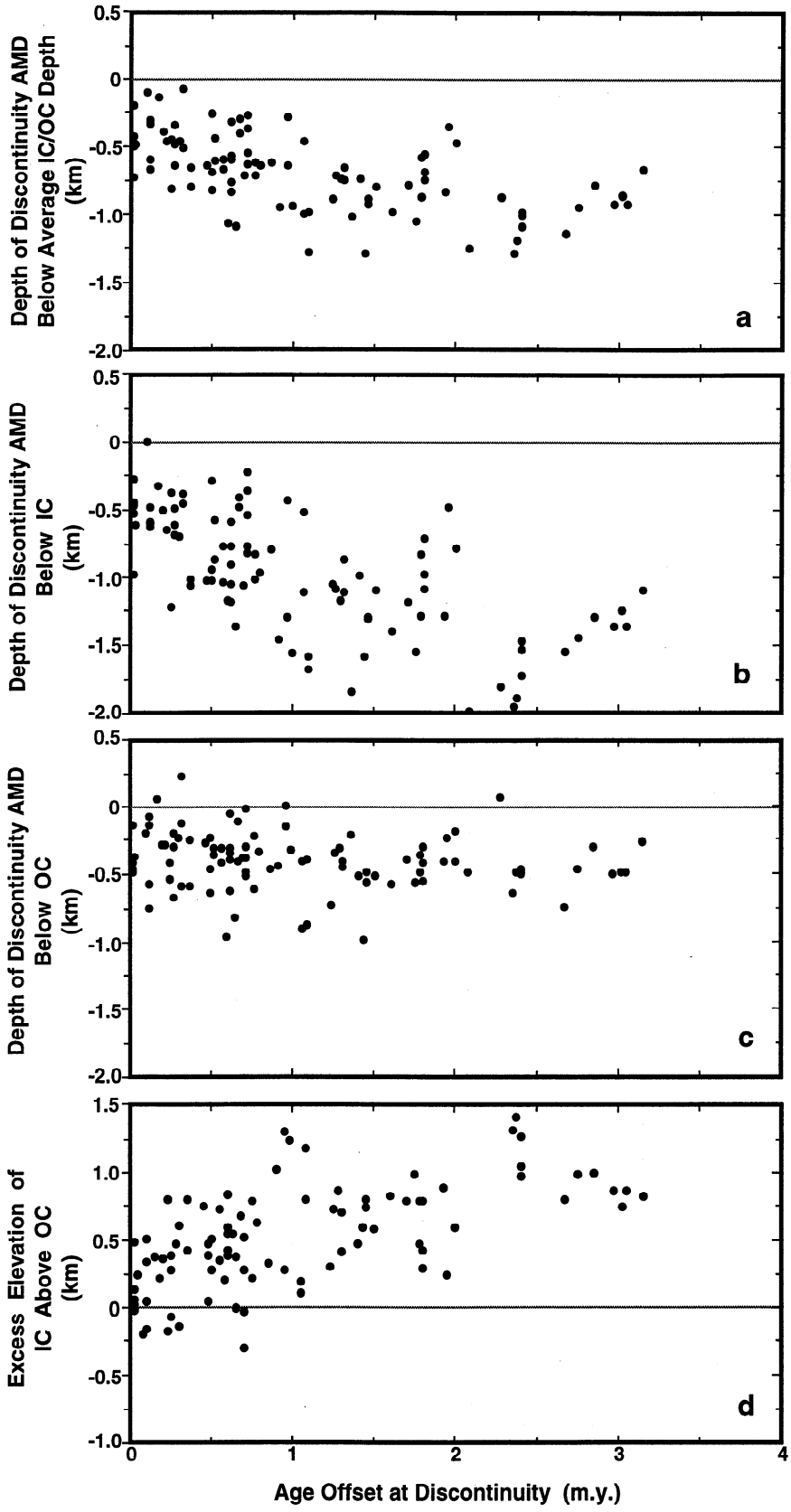

Figure 8. Relations between crustal depths in the vicinity of discontinuities and age offsets at the discontinuities. Each point is a 1-m.y. average of depth as described in Figure 7. All IC-OC depth comparisons are made along isochrons (comparison with discontinuity depth is made at the AMD midpoint between coeval isochrons in the adjacent segments). (a) Depth of discontinuity AMD below average depth of adjacent IC and OC crust (1/2[IC depth + OC depth]) versus age offset. (b) Depth of discontinuity AMD below depth of adjacent IC crust versus offset. (c) Depth of discontinuity AMD below depth of adjacent OC crust versus offset. (d) Elevation of IC crust above OC crust (on opposite side of discontinuity) versus offset.

onto IC crust, although the faults become increasingly irregular, more variably oriented, and have increased throw. These features are particularly pronounced close to the bounding discontinuities, forming a sharp contrast with the adjacent OC crust (e.g., Figure 5). Such OC to IC differences were noted throughout the Atlantic by *Tucholke and Lin* [1994], and they also have been demonstrated statistically by *Goff et al.* [1995] within our survey area. In near-axis (2-7 Ma) analysis of segments E, G, and H, *Goff et al.* [1995] documented increasing rms roughness and characteristic width of abyssal hills toward IC crust, as well as decreasing aspect ratios (elongation); over the run of segments C, D, and E from 29 to 2 Ma, typical rms roughness was found to be ~300-350 m on IC crust and only ~200-250 m on OC crust. Identification of fault scarps in HMR1 sidescan imagery (e.g., Figure 6) and comparison with seafloor morphology (Plate 1) shows that most of this abyssal-hill relief is caused by faulting.

A unique feature of IC crust is the common occurrence of large, elliptical to quasi-circular domes that rise immediately adjacent to the NTDs (Plate 1). Some of the best examples occur along the southern edges of (1) segment G at 46°25'W (Figures 9a and 9b), 46°50'W, and 47°38'W; (2) segment H at 45°35'W; and (3) segment E at 47°45'W (Figure 6). No comparable features are found in SC or OC crust. The domes usually are 10-20 km in diameter and have relief of up to 1-2 km. In HMR1 sidescan images the domes tend to exhibit diffuse backscatter as well as large, irregular normal faults and numerous, chaotically distributed smaller faults (Figure 6, top left and Figure 9b). Many of the faults, particularly the smaller ones, appear to be scars left by slides and slumps. Thus the domes may have had an original morphology that was somewhat smoother and more regular.

Differences among IC, SC, and OC crust also are readily apparent when we consider deeper structure suggested by gravity data. *Tucholke and Lin* [1994] and *Escartín and Lin* [1995] observed that IC crust in MAR near-axis settings tends to have high values of residual gravity, whereas SC and OC crust have low and intermediate values, respectively. This pattern is developed over the full run of the segments in our survey (Figure 3). Cross-isochron bands of high residual gravity generally follow the discontinuities between segments, but the axes of these bands are distinctly shifted about 10-15 km onto IC crust (i.e., onto the southern margins of most segments). In some places the axes of even subtle gravity highs show this displacement, for example just north of the small-offset C-D discontinuity (Figure 3). The pattern is also observed where a spreading segment has two inside corners. In segment G, both inside corners between anomalies 5E and 5AC (Figure 2) encompass the axes of residual gravity highs (Figure 3). When the NTD at the northern edge of segment G changed from left-stepping to zero offset at ~13.9 Ma, the northern part of the segment was no longer in an IC tectonic setting, and its residual gravity anomaly correspondingly became reduced. The NTD reappeared as a right-stepping offset at ~10.2 Ma; at this time the northern part of segment G assumed an OC position and had a moderate residual gravity anomaly, and the new IC crust in the adjacent, southern part of segment H encompassed the axis of a residual-gravity high (Figure 3).

It is well known that ocean crust is thin in both transform and nontransform discontinuities [*Detrick et al.*, 1993], and this is consistent with the relatively elevated residual gravity values observed along the discontinuities in our survey area. However, because the axes of the residual gravity highs are shifted to positions over IC crust, it follows that IC crust also is anomalously thin; in fact, it may be thinner than crust beneath the discontinuities. Relative crustal thickness along the gravity axes over IC crust, computed from residual gravity anomaly by *Lin et al.* [1993], averages 1-2 km thinner than crust beneath segment centers. This is probably a minimum difference. Recent comparisons of crustal thicknesses determined from refraction data and coincident gravity data by *Minshull* [1996] suggest that the gravity data consistently underestimate crustal-thickness variations.

The lowest residual gravity values are observed in cross-isochron bands over segment centers (Figure 3), and intermediate values commonly appear over OC crust. These observations are consistent with a pattern of thickest crust near segment centers, as suggested along the Mid-Atlantic Ridge axis both by gravity [*Kuo and Forsyth*, 1988; *Lin et al.*, 1990] and seismic refraction studies [*Tolstoy et al.*, 1993].

Temporal Variations

Aside from segment life span and evolution of segment lengths already noted, the principal temporal change in segments is a strong cross-isochron variation in residual gravity anomaly (Figure 3). Positive and negative anomalies have circular (bull's-eye) form or are elongated parallel to isochrons within the larger gravity bands that follow the run of segments. The relative gravity highs tend to line up along isochrons within segments, as do intervening lows. The cross-isochron variations have relatively consistent wavelength, and they suggest regular changes in crustal thickness every ~2-3 m.y. Peak-to-trough amplitudes in the residual gravity are ~5-15 mGal, implying changes of up to 1.5 km in crustal thickness as computed from the gravity data [*Lin et al.*, 1993]. As noted earlier, actual crustal-thickness variations may be larger.

Intersegment Variations

There are significant differences in character among the segments surveyed. The greatest contrasts are between segments E and G, which we summarize here. Segment E has the most consistent and predictable crustal morphology (Plate 1). Abyssal hills are very linear and have moderate to low amplitude; they commonly extend 30-50 km along isochrons, and in the youngest ~10 m.y. of seafloor most abyssal hills run the full length of the segment. Irregular, high-amplitude faults and elliptical domes characteristic of IC crust disrupt this structure only at the southernmost edge of the segment (Figure 6), indicating that the IC tectonic setting is very restricted. Residual gravity in segment E also is relatively low overall (Figure 3), suggesting mostly normal crustal thicknesses. Segment E is interpreted to be magmatically robust compared to other segments within the region.

In contrast, segment G exhibits higher-amplitude and more irregular topographic patterns (Plate 1). Linear abyssal hills are concentrated mostly in OC crust and rarely extend more than 20-30 km. From the segment center to IC crust, irregular large-throw faults commonly form the abyssal hills, and their strike varies from ridge-parallel to highly oblique. Large, quasi-circular domes are extensively developed along the southern, IC margin of the segment. Much of segment G is dominated by elevated residual gravity (Figure 3) and thus by apparently thin crust. It is particularly notable that the large

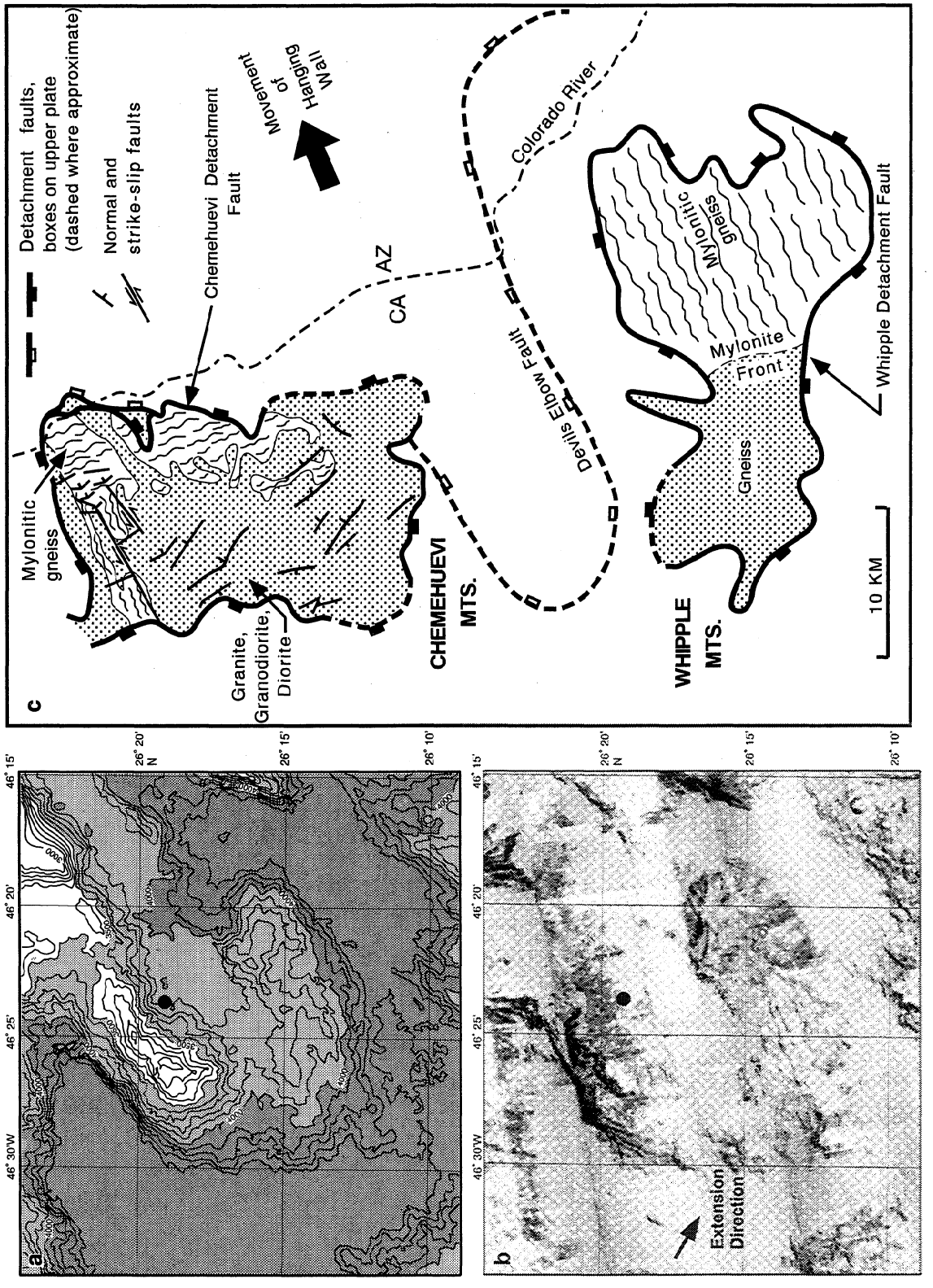

Figure 9. Plan-view comparison of submarine dome at IC edge of segment G (left) with "turtleback" metamorphic core complexes exposed in the Chemehuevi and Whipple mountains in southeastern California (right). All maps are at the same scale. (a) Bathymetry of the submarine dome; contours at 100-m intervals. Solid circle locates dredged serpentinite. (b) HMR1 sidescan-sonar image (southward insonification) of the same feature. (c) Highly simplified geological map of the subaerial metamorphic core complexes, adapted from *John* [1987] and *Yin and Dunn* [1992]. Both the submarine and subacrial features are thought to have originated by detachment faulting, and they have similar scales, roughly equidimensional to elliptical outlines, domed morphology, and internal occurrence of high-angle normal faults orthogonal to the direction of extension.

IC domes are consistently associated with the most elevated residual gravity anomalies and presumed thinnest crust. Segment G is interpreted to have had a history of very limited magmatism compared to the other spreading segments.

Discussion

Controls on Segmentation

The 29-m.y. record of crustal structure in our survey shows that spreading segments can be long-lived features of the plate boundary, even where separated by only very small to zero-offset discontinuities. The evolution of these segments helps to constrain the hypotheses of magmatic versus tectonic control of segmentation pattern. According to the magmatic hypothesis, segments are positioned above rising melt diapirs [*Whitehead et al.*, 1984] or mantle upwelling centers [*Lin et al.*, 1990] which have relatively fixed spacing in the subaxial asthenosphere. Previous aeromagnetic and seismic observations over old, sediment-covered seafloor in the North Atlantic [*Schouten and White*, 1980; *Schouten and Klitgord*, 1982] suggest that this spacing is maintained even though active upwelling may be episodic. Our data provide much more complete structural information with which to test this idea. The data show that the G-H and H-I discontinuities disappeared for up to 3-4 m.y. during periods of zero offset (~13.9-10.2 Ma and 10.2-7 Ma), but they then reappeared at the same locations along the plate boundary (Figure 2). Another example of segment-boundary stability in the absence of significant offset is found in the young part of the H-I discontinuity, where the offset has been near zero over the past 5 m.y. (Plate 1 and Figure 2). Thus segments G, H, and I have maintained their integrity for the past ~14 m.y. even though thermal and mechanical perturbations at their boundaries were weak or absent. The persistence of this segmentation suggests that there are deep-seated, asthenospheric controls on segment position and longevity, as predicted by the magmatic hypothesis.

In contrast to the magmatic hypothesis, the tectonic hypothesis suggests that segment position and longevity are controlled by the configuration of mechanical discontinuities in the lithosphere [*Mutter and Karson*, 1992]. Rheological memory of discontinuities is required to produce coherent evolution of segments, and this memory probably is provided by the thermal-edge effect and the mechanical weakness of sheared lithosphere at the offsets [e.g., *Fox and Gallo*, 1984]. Both of these factors contribute to the stability of large-offset transform faults and the quasi-stability of smaller offsets, but when discontinuities evolve to zero offset, their rheological memory is lost. Therefore, according to the tectonic hypothesis, there is no reason for a discontinuity to reappear at its former ridge-axis position after a long period of zero offset. This is inconsistent with the observed evolution of the G-H and H-I discontinuities.

The evolution of plate-boundary structure at the time of the large, ~9° change in relative plate motion about 24-22 Ma also provides insight into the possible role of lithosphere mechanics. Prior to the plate-motion change, the C-D discontinuity was a small (≤5 km), right-stepping offset. The change in plate motion should have caused CCW rotation of spreading axes in segments C and D, thus lengthening the C-D offset and enhancing the offset's thermal and mechanical signature (Figure 10a). Instead, the offset disappeared (Figure 10b) and left no seafloor structural trace or gravity signature (Plate 1 and Figure 3), again indicating that the segmentation was not controlled simply by lithosphere mechanics. (The right-stepping B-C offset also disappeared, but the demise of

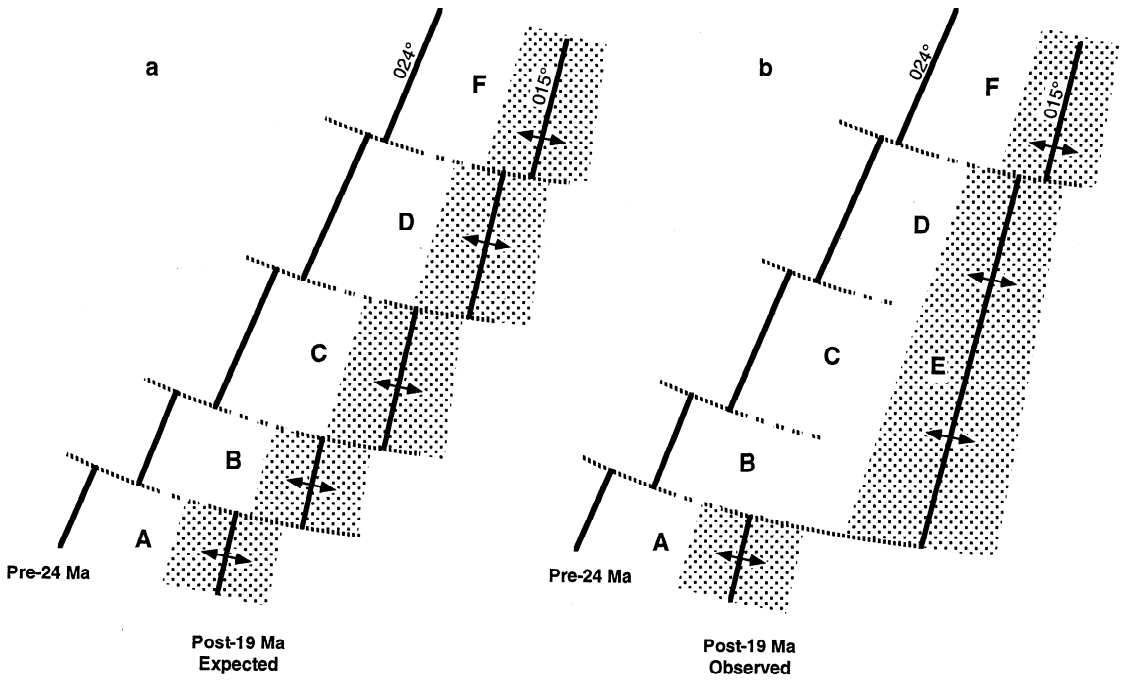

Figure 10. Sketch showing evolution of nontransform discontinuities across the large CCW change in relative plate motion that began ~24 Ma. Segments are lettered as in Figures 2 and 3. (a) Expected change: CCW rotation of spreading axes lengthens offsets at NTDs and augments their structural and thermal perturbations. (b) Observed change: strongly asymmetric spreading or ridge jumps eliminated the C-D and B-C discontinuities, and their structural and geophysical signatures disappeared.

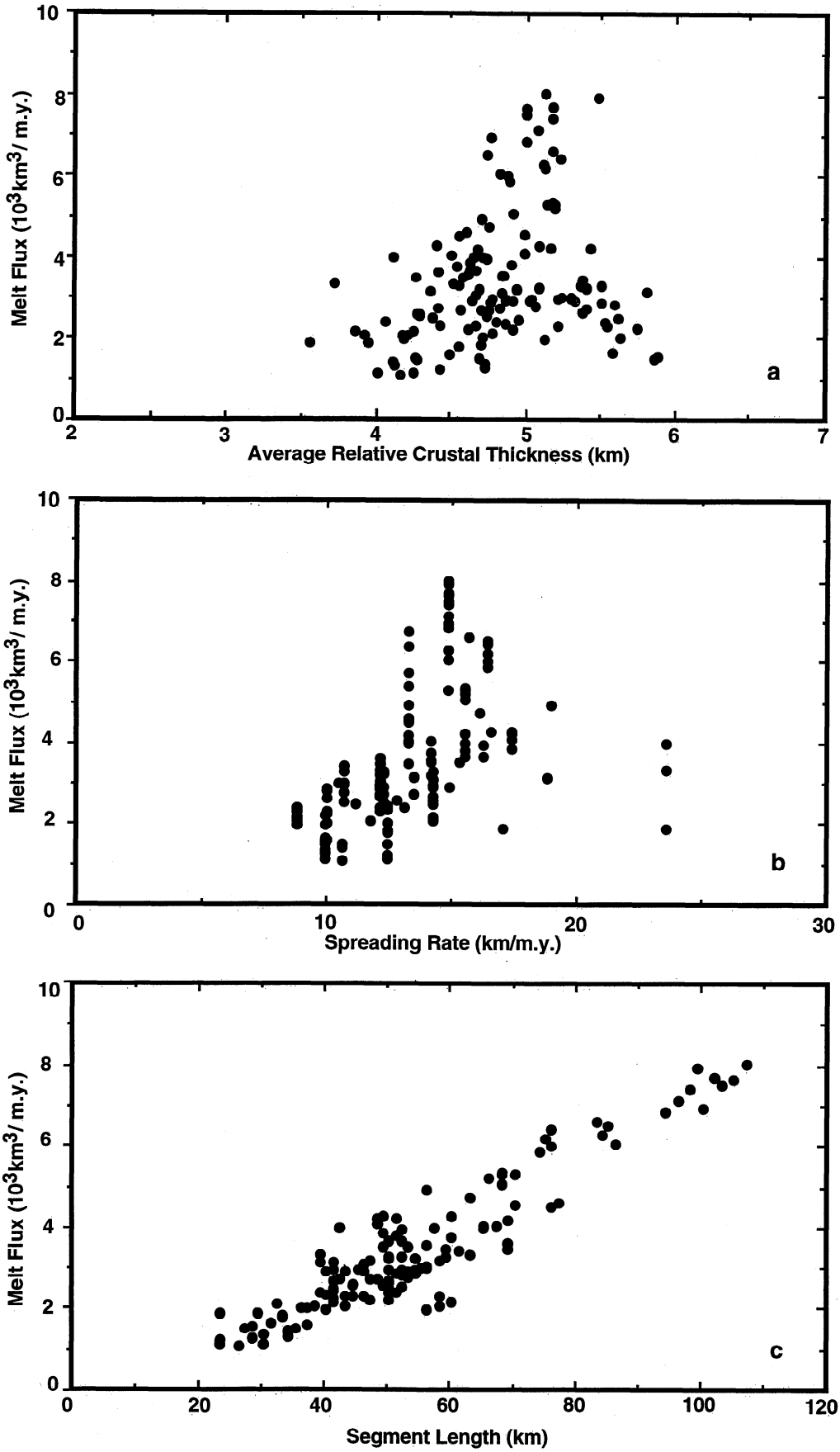

Figure 11. Plots of melt flux versus (a) crustal thickness, (b) spreading rate, and (c) segment length. Data points represent average segment length, width (across isochrons), relative crustal thickness, and relative crustal volume determined along linear approximations of isochrons in 0.5-m.y. bins over the run of each segment.

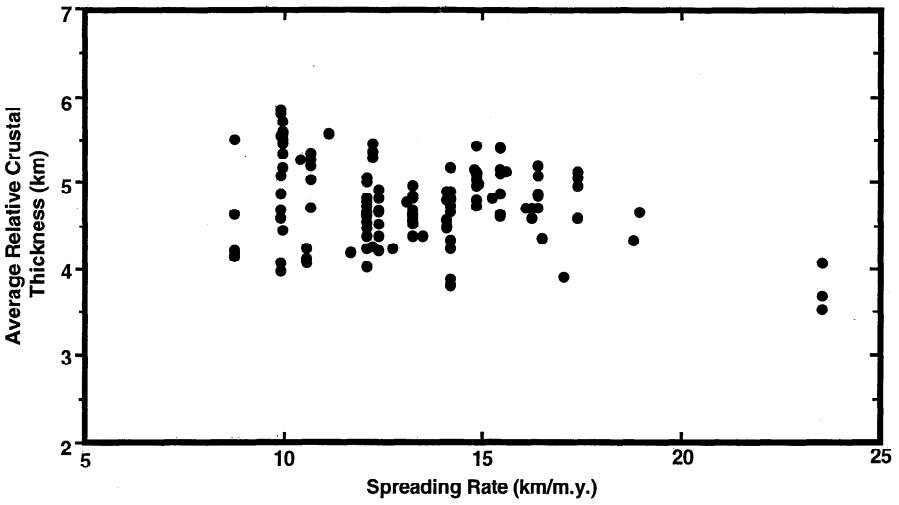

Figure 12. Plot of apparent crustal thickness versus spreading rate, with data points determined in 0.5-m.y bins as in Figure 11. Note the slight trend of decreasing crustal thickness with increasing spreading rate.

segment B may be related to capture by the northward migrating A-B discontinuity).

On the other hand, there are instances where lithosphere mechanics appear to be important. The division of segment F into segments G and H at the time of the major plate-motion change is a case in point. It is improbable that two new upwelling centers developed just at the time of the plate-motion change to form the new spreading segments. Instead, the division of segment F appears to have been a mechanical response of the plate boundary to the change in spreading direction. From these observations on segment evolution, we consider it likely that deep-seated magmatic processes play a dominant role in controlling segment position and longevity, although lithosphere mechanics is probably also important in initiating segmentation, and it may even control segment evolution if the upwelling signal is weak.

The magmatic and tectonic hypotheses can also be examined in terms of the relations between melt flux from the mantle (assumed to be equal to the apparent volume of crust accreted per unit time) and segment dimensions. These parameters are plotted in Figure 11, and they incorporate relative crustal thicknesses calculated from the residual gravity field [*Lin et al.*, 1993]. This calculation of course does not provide absolute crustal thicknesses, and the apparent crustal thicknesses may be affected by factors such as the presence of low-density serpentinized mantle. However, the results do give a first-order approximation of crustal-thickness variations that can be used to examine relative changes of crustal volume through time within segments.

According to the tectonic hypothesis, melt flux from passively upwelling mantle should vary in proportion to spreading rate and segment length but be independent of crustal thickness, which should be relatively constant. The magmatic hypothesis (active mantle upwelling) suggests that crustal thickness and segment length should vary in proportion to melt flux, while spreading rate (controlled by long-period changes in plate motion) and melt flux should vary independently. Melt flux is observed to vary with segment length (Figure 11c) as expected in both hypotheses, but comparisons of melt flux with crustal thickness and spreading rate (Figures 11a and 11b) show large scatter and no clear trends that would discriminate between the hypotheses. The scatter probably is produced by a combination of factors, including melting of heterogeneous mantle, errors in the gravity-derived crustal thicknesses, and flank-to-flank asymmetries in crustal accretion. A different approach is to compare crustal thickness against spreading rate (Figure 12). With passive upwelling, crustal thickness should remain constant over changes in spreading rate, whereas with active upwelling, crustal thickness should increase with decreasing spreading rate. The latter trend, although weakly developed, is observed in Figure 12 and tends to support the magmatic hypothesis.

We conclude that the data on melt flux versus segment dimensions, like the independent data on plate-boundary evolution discussed previously, favor deep-seated magmatic processes as the primary control on segmentation. We point out, however, that the melt-flux observations suffer from significant uncertainties because they are based on gravity-derived crustal thicknesses. True crustal thicknesses must be better determined in a representative sample of varying segment lengths and spreading rates before these observations can be adequately tested.

Structure of Spreading Segments

There are first-order differences in crustal structure of IC, SC, and OC tectonic settings. IC crust on the old sides of discontinuities is consistently elevated above coeval OC crust on the young sides of the discontinuities (Figures 7), and this asymmetry increases with magnitude of age offset for offsets up to at least 3 m.y. (Figure 8d). *Severinghaus and Macdonald* [1988] compiled ridge-axis data on IC/OC asymmetry versus age offset for offsets of up to 40 m.y., and their plots show an apparently similar trend but with very strong scatter. The origin of the depth asymmetry remains uncertain. Both dynamic and static effects have been proposed (see summary by *Tucholke and Lin* [1994]), and they generally are related to the observations that IC and OC crust most likely have compositional differences or that IC crust, unlike OC crust, is edged by two weak boundaries (rift axis and active discontinuity). Recently, *Pockalny et al.* [1996] suggested that elevated transverse ridges form in IC crust as a flexural response to

extension (normal to discontinuity) induced by plate-motion changes. Whatever the actual mechanism of uplift near the ridge axis, it creates a depth offset that is locked into the structure of the discontinuity for at least 20-30 m.y. (Figure 7).

Asymmetry in residual gravity signature is also pronounced (Figure 3), and it suggests a pattern of thin, thick, and intermediate-thickness crust in IC, SC, and OC tectonic settings, respectively. This signature is quite sensitive to sense of offset at a discontinuity, even when offsets are small or temporary; the elevated and apparently thin IC crust that formed south of the small, left-stepping G-H discontinuity between anomalies 5E and 5AC is a good example (Figures 2 and 3 and Plate 1). Similar IC/OC asymmetry in residual gravity also can be observed in other off-axis surveys in the North Atlantic (e.g., SARA and Atlantis FZ, Figure 1 [*Rommevaux et al.*, 1994; *Pariso et al.*, 1995]). It is less well developed in the area of the SEADMA I cruise south of Kane FZ [*Gente et al.*, 1995] where NTDs generally have small offsets (<10 km). However, dredging in this region by *Cannat et al.* [1995] demonstrated that gabbroic and ultramafic rocks are consistently exposed in locations where residual gravity highs are present near the NTDs. In our survey area, dredging at the IC edge of segment G recovered small quantities of basalt at five locations; serpentinized peridotite was recovered at a sixth location, on the IC dome and associated strong positive residual gravity anomaly near 46°25'W (Figures 3, 9a, and 9b). These off-axis recoveries of gabbros and mantle ultramafics, together with similar near-axis observations [*Tucholke and Lin*, 1994], confirm that thin crust is associated with residual gravity highs along the run of inside corners.

We interpret the crustal thinning at inside corners to be caused by low-angle, detachment faulting near segment ends at the spreading axis [e.g., *Dick et al.*, 1981; *Karson*, 1990; *Tucholke and Lin*, 1994]. The inside corner constitutes the footwall of the detachment fault, and crust in the rift-valley floor is the hanging wall. Melt is intruded into and extruded onto the hanging wall to form a relatively normal crustal section that is transported to the outside corner. The IC footwall typically exposes lower crustal to upper mantle rocks exhumed from deep beneath the spreading axis. As the IC lithosphere is uplifted into the rift mountains, it becomes dissected by high-angle normal faults.

The character of high-angle normal faults appears to vary with crustal thickness. Thin IC crust exhibits large-throw, irregular faults and large abyssal hills, whereas thicker crust in both SC and OC settings displays long, linear faults and abyssal hills of moderate amplitude. Similar contrasts are observed at intersegment scales; segment E has relatively normal-thickness crust overall and has experienced uniform faulting of moderate amplitude (Plate 1), whereas the apparently thinner crust of segment G is characterized by higher-amplitude, irregular faults. The contrasts also appear over the run of individual segments. In segment E, for example, crust between anomalies ~5Br and 3Ar exhibits both the highest residual gravity anomaly (thinnest crust) and the most irregular, high-amplitude faults and abyssal hills within the segment (Figures 2 and 3 and Plate 1 [see also *Goff et al.*, 1995, Figure 10]). At much larger, interocean-basin scales, high-amplitude faults and abyssal hills are known to develop with decreasing spreading rate and reduced magma budget [e.g., *Macdonald*, 1982]. Our results suggest that this same correlation applies at the smaller, intersegment and intrasegment scales. A thermal-mechanical explanation for a link between crustal thickness and spacing/throw of faults is discussed by *Shaw and Lin* [1996].

Magmatic Versus Amagmatic Extension

The 2- to 3-m.y. variation in residual gravity anomaly is a prominent signal along the run of segments (Figure 3). Similar variations appear in the gravity field in other surveys along the northern Mid-Atlantic Ridge (Atlantis FZ, SARA, and SEADMA I; see Figure 1). It is difficult to explain these features by changes in upper mantle density, and they are thought to indicate real crustal thickening and thinning. We interpret the variations to be caused by cyclic (although not necessarily periodic) changes in the volume of melt input to the ridge axis through time. During episodes of high melt flux, crust of normal thickness would be formed, but during episodes of low melt flux, thinner crust would be emplaced, and the cooler lithosphere would also be more strongly extended by brittle strain on normal faults.

With such episodic melt input, we expect to see an approximate symmetry in residual gravity anomaly on the eastern ridge flank, conjugate to our survey. We currently do not have the east flank data to test this inference, but studies of conjugate crustal parcels to ~10 m.y. off axis made by *Rommevaux et al.* [1994], *Pariso et al.* [1995], and *Gente et al.* [1995] can be examined in this context. Figure 13 shows residual gravity anomaly versus age and gravity-derived crustal thickness versus age for west and east flank profiles along the midpoints of the four spreading segments south of Atlantis FZ. In three of these profiles there is reasonably good cross-axis symmetry, but the 29°10'N profile shows poor correlation between the two ridge flanks. In three other segments north of Atlantis FZ [*Pariso et al.*, 1995] and in segments to the south of Kane FZ [*Gente et al.*, 1995], residual gravity and crustal thickness variations are symmetrical only locally. Tempering our expectation of symmetry, we must recognize that crustal accretion at slow spreading ridges probably is not a normally symmetric process. Studies of the MAR axial valley by *Macdonald* [1977] and *Kleinrock and Humphris* [1996] show that the position and extent of the crustal-accretion zone can change widely over time within the confines of the rift-valley floor, creating asymmetries at scales of up to 10 km or more (~1 m.y. at observed spreading rates). Any persistent cross-rift asymmetry in tectonic versus magmatic extension could generate significantly skewed crustal-thickness and residual gravity patterns at even longer timescales.

If episodic magmatic versus relatively amagmatic extension is a viable explanation for the observed variations in apparent crustal thickness, there are two likely mechanisms by which this variation might be accomplished. In one, changes in partial melting caused by upwelling of heterogeneous mantle could lead to variable melt input to the rift valley. The typical wavelength of the crustal-thickness cycles is 30-40 km, and a similar scale would be expected for the mantle heterogeneities. Small (<100 km) mantle heterogeneities have been documented elsewhere on the MAR [*Bonatti et al.*, 1992], and they could be responsible for at least some segment-scale perturbations in melt flux [*Michael et al.*, 1994]. A possible drawback of this mechanism is that the observed temporal variation in apparent crustal thickness is quite regular (2-3 m.y.), and it seems unlikely that mantle heterogeneities would be scaled so consistently. Another possible mechanism is episodic formation of buoyant melt diapirs. If melting tends to be focused in deep-seated, quasi-regular insta-

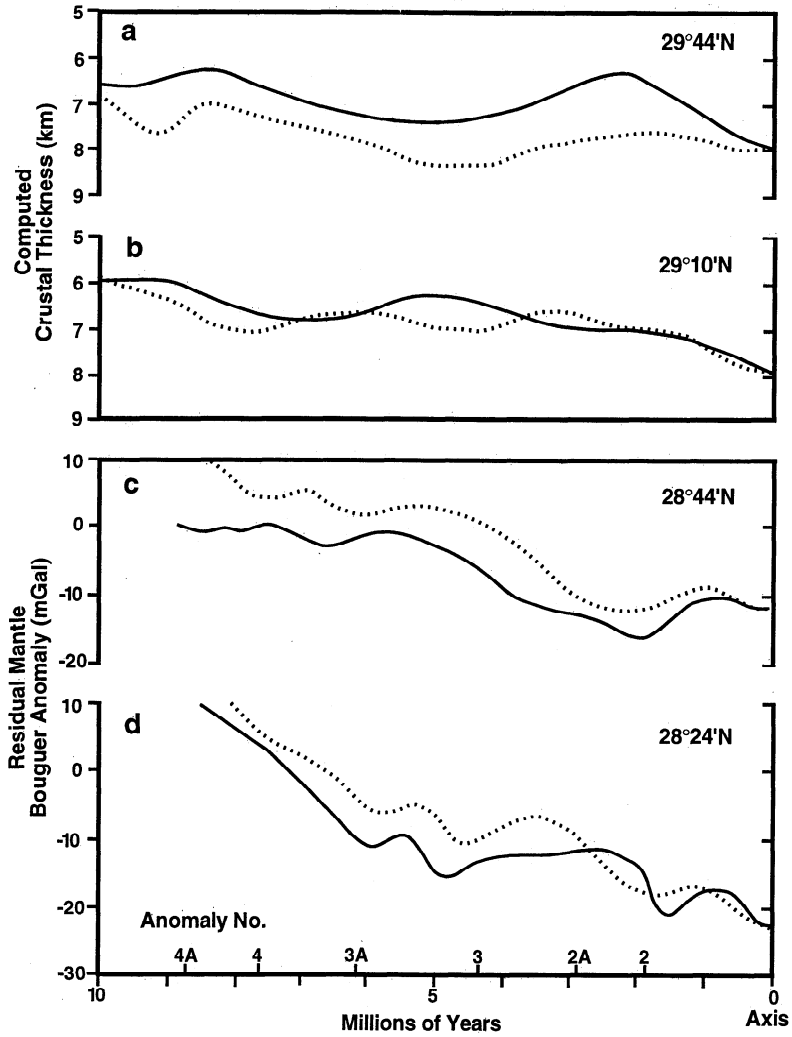

Figure 13. (a) and (b) Profiles of computed crustal thickness versus age along midpoints of two spreading segments immediately south of Atlantis FZ (adapted from *Pariso et al.* [1995]). (c) and (d) Profiles of residual mantle Bouguer anomaly versus age along midpoints of the next two spreading segments to the south (picked from maps of *Rommevaux et al.* [1994] following their traces of segment midpoints). West flank profiles are solid lines and conjugate east flank profiles are dashed lines.

bilities beneath segment midpoints [*Whitehead et al.*, 1984], melt may accumulate within the mantle and then episodically develop pathways to break through to the crust and seafloor. These two mechanisms should generate different geochemical signatures in the ocean crust, but appropriate geochemical data are not yet available to address this question.

We expect that during the amagmatic part of a crustal-accretion cycle, brittle extension will be enhanced and detachment faulting near segment ends probably will be best developed. This appears to be the case for the large, quasi-circular domes developed along the IC portions of spreading segments, particularly those at the southern margin of segment G (Plate 1). These features are regularly associated with along-isochron zones of elevated residual gravity anomaly, which suggest thin crust and limited melt input over the full length of the segment. The residual gravity anomalies over the features themselves are usually the highest within the survey area. We therefore interpret these domes as consisting of lower crustal and/or upper mantle rocks that were exposed by robust detachment faulting during relatively amagmatic phases of spreading.

There is an interesting analogy between the IC domes observed in our study area and metamorphic core complexes that have been studied in the Basin and Range of the western United States (Figure 9) [e.g., *Howard and John*, 1987; *Davis and Lister*, 1988]. Both kinds of features appear to originate by low-angle normal faulting, they expose rocks from unusually deep levels in the lithosphere, and they often have similar "turtleback" shapes. Their dimensions also are quite similar, typically in the range of 10-40 km for the exposed metamorphic core complexes, compared to 10-20 km for the domes observed on the MAR flank. In the Whipple core complex (Figure 9c) the transition from ductile to brittle deformation is well exposed in a mylonite front; during an amagmatic phase in slow spreading ocean crust, the deepening detachment fault could exhume mantle peridotites at inside corners within 0.3-0.6 m.y. [*Tucholke and Lin*, 1994], thus also potentially exposing the petrologic Moho, the rock record of melt generation and migration, and the record of ductile-brittle deformation in the ridge-axis lithosphere. Geological relations and structural scales observed in subaerial metamorphic core complexes may prove to be very useful for interpreting structure of

the submarine domes within the context of both regional geophysics and the typically very limited near-seafloor data that may be available.

Conclusions

We conducted a detailed survey of spreading segments that are bounded by mostly nontransform discontinuities in 0 to 29 Ma crust on the western flank of the Mid-Atlantic Ridge. Observed evolution of the segments helps to constrain hypotheses about controls on segment position and longevity, and intrasegment and intersegment structure shows consistent patterns that relate to patterns of melt supply and tectonism at the ridge axis. We conclude the following:

1. Segments along the slow spreading Mid-Atlantic Ridge can be long-lived, surviving for tens of millions of years. Some NTDs between segments alternated between small right- and left-stepping offset and even had long periods (3-4 m.y.) with zero offset, yet the spreading segments persisted along the plate boundary. During the changes in offset, the structural and thermal expression of the NTDs was markedly weakened or eliminated, suggesting that the presence of a mechanical discontinuity in the lithosphere is not a primary control on the position or long-term survival of the segments. The NTDs have not been fixed in position along the spreading axis but have migrated independently of one another.

2. A major change (~9°) in relative plate motion occurred about 24-22 Ma and caused a reorganization in plate-boundary segmentation. Over a period of about 3-4 m.y. one segment (F) was divided into two, two other segments (C and D) consolidated to form a new, long (~100 km) segment, and another segment (B) was eliminated. These changes were not simultaneous but proceeded from north to south. NTDs that geometrically should have been augmented by the plate-motion change were instead eliminated, again indicating that lithosphere mechanics is not solely responsible for plate-boundary segmentation. However, during a plate-motion change, new discontinuites also can appear, apparently as a purely mechanical response of the plate boundary to the new orientation of plate stresses.

3. Our observations are consistent with the hypothesis that locations and longevity of spreading segments bounded by NTDs are controlled primarily by buoyant upwelling of asthenosphere or melt near segment centers (the magmatic hypothesis). Segment length appears to be strongly correlated with melt flux to the segment. Taken in the context of the magmatic hypothesis, this observation suggests that segment length is controlled by the volume of supplied melt. In the same context, the observed migration of spreading segments indicates that the governing plume locations are not fixed in the asthenosphere but also must migrate.

4. There are consistent differences in depth, morphology, residual gravity anomaly, and apparent crustal thickness among IC, SC, and OC tectonic settings within segments. Residual gravity anomalies suggest that segment centers have the thickest crust and OC settings have intermediate-thickness crust. Compared to OC locations, IC lithosphere is shallower, has more irregular and higher-amplitude faulting and abyssal hills, exhibits higher residual gravity anomalies (and thus has apparently thinner crust), and is prone to expose lower crust and upper mantle at the seafloor. This striking asymmetry is interpreted to be caused by low-angle, detachment faulting near segment ends at the spreading axis, with OC lithosphere defining the hanging wall and IC lithosphere comprising the footwall.

5. Amplitude of fault throw and height of abyssal hills increase with increasing residual gravity value and thus with decreasing apparent crustal thickness. Within segments, this is observed in differences between IC and OC crust, but it is also observed over long periods (~5-10 m.y.) along the run of segments (e.g., in segment E). Similar relations apply at the intersegment scale when relatively amagmatic segments (segment G) and more magmatic segments (segment E) are compared. These intrasegment and intersegment relations are consistent with the large-scale, more global observation that mid-ocean ridge topography is spreading-rate (melt supply) dependent.

6. Residual gravity variations suggest that episodic crustal thickening and thinning occurs over the run of segments at intervals of 2-3 m.y. We attribute this variation to cyclic changes in melt input caused by episodic melt release from the upwelling asthenosphere. The regularity of the cycles suggests that this release is not controlled by changes in partial melting of randomly heterogeneous mantle but rather that melt may be accumulated in the mantle until it quasiperiodically breaks through to the rift-axis crust. Dome-like edifices of lower crustal and upper mantle rocks develop at the IC edges of segments during periods of relatively amagmatic spreading, probably because of enhanced brittle extension on low-angle, detachment faults. The domes are analogous to "turtleback" metamorphic core complexes exposed in subaerial environments, and the geology of the subaerial features may provide significant insights into the origin and structure of their submarine counterparts.

Acknowledgments. We thank M. Orr, M. Badiey, and J. Kravitz for their long-standing support of the geological and geophysical studies in the ONR Atlantic Natural Laboratory. We are indebted to the following for their seagoing and laboratory contributions to this study: W.K. Stewart, J. Howland, and M. Marra for sonar processing; M. Edwards and the technical staff of the HMR1 Mapping Group for HMR1 acquisition and processing; and the scientific staff, technical staff, and officers and crew of R/V *Ewing Cruise* 92-08 for their strong contributions to successful seagoing operations. We also thank P. Lemmond and L. Dolby for assistance with programming, data processing, and graphics; G. Hirth, H. Dick, and J. Escartín for helpful discussions; and D. Naar, J. Madsen, and D. Toomey for reviews of the manuscript. This research was supported by ONR grants N00014-90-J-1621 and N00014-94-1-0466 and NSF grant OCE-9300708. Contribution 9375 of Woods Hole Oceanographic Institution.

References

Bhattacharyya, B. K., Two-dimensional harmonic analysis as a tool for magnetic interpretation, *Geophysics, 30,* 829-857, 1965.

Bonatti, E., A. Peyve, P. Kepezhinskas, N. Kurentsova, M. Seyler, S. Skolotnev, and G. Udintsev, Upper mantle heterogeneity below the Mid-Atlantic Ridge, 0°-15°N, *J. Geophys. Res., 97,* 4461-4476, 1992.

Cande, S. C., and D. V. Kent, A new geomagnetic polarity timescale for the Late Cretaceous and Cenozoic, *J. Geophys. Res., 97,* 13,917-13,951, 1992.

Cannat, M., et al., Thin crust, ultramafic exposures, and rugged faulting patterns at the Mid-Atlantic Ridge (22°-24°N), *Geology, 23,* 49-52, 1995.

Carbotte, S. M., S. M. Welch, and K. C. Macdonald, Spreading rates, rift propagation, and fracture zone offset histories during the past 5 my on the Mid-Atlantic Ridge; 25°-27°30'S and 31°-34°30'S, *Mar. Geophys. Res., 13,* 51-80, 1991.

Caress, D. W., and D. N. Chayes, Improved processing of Hydrosweep DS multibeam data on the R/V Maurice Ewing, *Mar. Geophys. Res., 18,* 631-650, 1996.

Collette, B. J., and W. R. Roest, Further investigations of the North

Atlantic between 10° and 40°N and an analysis of spreading from 118 Ma ago to present, *Proc. K. Ned. Akad. Wet., 95,* 159-206, 1992.

Crane, K., The spacing of ridge-axis highs: Dependence upon diapiric processes in the underlying asthenosphere?, *Earth Planet. Sci. Lett., 72,* 405-414, 1985.

Davis, G. A., and G. S. Lister, Detachment faulting in continental extension: Perspectives from the southwestern U.S. Cordillera, *Spec. Pap. Geol. Soc. Am., 218,* 133-159, 1988.

Detrick, R. S., R. S. White, and G. M. Purdy, Crustal structure of North Atlantic fracture zones, *Rev. Geophys., 31,* 439-458, 1993.

Detrick, R. S., H. D. Needham, and V. Renard, Gravity anomalies and crustal thickness variations along the Mid-Atlantic Ridge between 33°N and 40°N, *J. Geophys. Res., 100,* 3767-3787, 1995.

Dick, H. J. B., G. Thompson, and W. B. Bryan, Low angle faulting and steady-state emplacement of plutonic rocks at ridge-transform intersections (abstract), *Eos Trans. AGU, 62*(17), 406, 1981.

Dick, H. J. B., H. Schouten, P. S. Meyer, D. G. Gallo, H. Bergh, R. Tyce, P. Patriat, K. T. M. Johnson, J. Snow, and A. Fisher, Tectonic evolution of the Atlantis II Fracture Zone, in *Proceedings of the Ocean Drilling Program, Scientific Results,* vol. 118, edited by R. P. Von Herzen and P. T. Robinson, pp. 359-398, Ocean Drill. Program, College Station, Tex., 1991.

Escartín, J., and J. Lin, Ridge offsets, normal faulting, and gravity anomalies of slow spreading ridges, *J. Geophys. Res., 100,* 6163-6177, 1995.

Fox, P. J., and D. G. Gallo, A tectonic model for ridge-transform-ridge plate boundaries: Implications for the structure of oceanic lithosphere, *Tectonophysics, 104,* 205-242, 1984.

Frey, F. A., D. Stakes, N. Walker, S. R. Hart, and R. Nielsen, Geochemical characteristics of basaltic glasses from the AMAR and FAMOUS axial valleys, Mid-Atlantic Ridge (36°-37°N): Petrogenetic implications, *Earth Planet. Sci. Lett., 115,* 117-136, 1993.

Gente, P., R. A. Pockalny, C. Durand, C. DePlus, M. Maia, G. Ceuleneer, C. Mével, M. Cannat, and C. Laverne, Characteristics and evolution of the segmentation of the Mid-Atlantic Ridge between 20°N and 24°N during the last 10 million years, *Earth Planet. Sci. Lett., 129,* 55-71, 1995.

Goff, J. A., B. E. Tucholke, J. Lin, G. E. Jaroslow, and M. C. Kleinrock, Quantitative analysis of abyssal hills in the Atlantic Ocean: A correlation between inferred crustal thickness and extensional faulting, *J. Geophys. Res., 100,* 22,509-22,522, 1995.

Grindlay, N. R., P. J. Fox, and K. C. Macdonald, Second-order ridge axis discontinuities in the South Atlantic: Morphology, structure, evolution, *Mar. Geophys. Res., 13,* 21-49, 1991.

Howard, K. A., and B. E. John, Crustal extension along a rooted system of imbricate low-angle faults: Colorado River extensional corridor, California and Arizona, *Geol. Soc. Spec. Publ. 28,* 299-311, 1987.

International Association of Geomagnetism and Aeronomy (IAGA), Division I, Working Group 1, International geomagnetic reference field revision 1987, *IAGA News, 26,* 87-92, 1987.

John, B. E., Geometry and evolution of a mid-crustal extensional fault system: Chemehuevi Mountains, southeastern California, *Geol. Soc. Spec. Publ. 28,* 313-335, 1987.

Karson, J. A., Seafloor spreading on the Mid-Atlantic Ridge: Implications for the structure of ophiolites and oceanic lithosphere produced in slow-spreading environments, in *Proceedings of the Symposium TROODOS 1987,* edited by J. Malpas, et al., pp. 547-555, Geol. Surv. Dep., Nicosia, Cyprus, 1990.

Karson, J. A., and H. J. B. Dick, Tectonics of ridge-transform intersections at the Kane Fracture Zone, *Mar. Geophys. Res., 6,* 51-98, 1983.

Kleinrock, M. C., and S. E. Humphris, Structural asymmetry of the TAG rift valley: Evidence from a near-bottom survey for episodic spreading, *Geophys. Res. Lett., 23,* 3439-3442, 1996.

Klitgord, K. D., Sea-floor spreading: The central anomaly magnetization high, *Earth Planet. Sci. Lett., 29,* 201-209, 1976.

Kuo, B. Y., and D. W. Forsyth, Gravity anomalies of the ridge-transform system in the South Atlantic between 31° and 34.5°S: Upwelling centers and variations in crustal thickness, *Mar. Geophys. Res., 10,* 205-232, 1988.

Lachenbruch, A. H., and G. A. Thompson, Oceanic ridges and transform faults: Their intersection angles and resistance to plate motion, *Earth Planet. Sci. Lett., 15,* 116-122, 1972.

Lin, J., G. M. Purdy, H. Schouten, J.-C. Sempéré, and C. Zervas, Evidence from gravity data for focused magmatic accretion along the Mid-Atlantic Ridge, *Nature, 344,* 627-632, 1990.

Lin, J., B. E. Tucholke, and M. C. Kleinrock, Off-Axis "boudin-shaped" gravity lows on the western flank of the Mid-Atlantic Ridge at 25°25'-27°10'N: Evidence for long-term pulses in magmatic accretion in spreading segments (abstract), *Eos Trans. AGU, 74*(16), Spring Meet. Suppl., 380, 1993.

Macdonald, K. C., Near-bottom magnetic anomalies, asymmetric spreading, oblique spreading, and tectonics of the Mid-Atlantic Ridge near lat 37°N, *Geol. Soc. Am. Bull., 88,* 541-555, 1977.

Macdonald, K. C., Mid-ocean ridges: Fine scale tectonic, volcanic, and hydrothermal processes within the plate boundary zone, *Annu. Rev. Earth Planet. Sci., 10,* 155-190, 1982.

Macdonald, K. C., The crest of the Mid-Atlantic Ridge: Models for crustal generation processes and tectonics, in *The Geology of North America,* vol. M, *The Western North Atlantic Region,* edited by P. R. Vogt and B. E. Tucholke, pp. 51-68, Geol. Soc. of Am., Boulder, Colo., 1986.

Macdonald, K. C., R. M. Haymon, and S. P. Miller, Deep-tow and Sea Beam studies of dueling propagating ridges on the East Pacific Rise near 20°40'S, *J. Geophys. Res., 93,* 2875-2898, 1988.

McNab, R., J. Verhoef, W. Roest, and J. Arkani-Hamed, New database documents the magnetic character of the Arctic and North Atlantic, *Eos Trans. AGU, 76*(45), 449, 458, 1995.

Menard, H. W., and T. M. Atwater, Changes in direction of sea floor spreading, *Nature, 219,* 463-467, 1968.

Michael, P. J., et al., Mantle control of a dynamically evolving spreading center: Mid-Atlantic Ridge 31-34°S, *Earth Planet. Sci. Lett., 121,* 451-468, 1994.

Minshull, T. A., Along-axis variations in oceanic crustal density and their contribution to gravity anomalies at slow-spreading ridges, *Geophys. Res. Lett., 23,* 849-852, 1996.

Müller, R. D., and W. R. Roest, Fracture zones in the North Atlantic from combined Geosat and Seasat data, *J. Geophys. Res., 97,* 3337-3350, 1992.

Mutter, J. C., and J. A. Karson, Structural processes at slow-spreading ridges, *Science, 257,* 627-634, 1992.

Pariso, J. E., J.-C. Sempéré, and C. Rommevaux, Temporal and spatial variations in crustal accretion along the Mid-Atlantic Ridge (29°-31°30'N) over the last 10 m.y.: Implications from a three-dimensional gravity study, *J. Geophys. Res., 100,* 17,781-17,794, 1995.

Parker, R. L., The rapid calculation of potential anomalies, *Geophys. J. R. Astron. Soc., 31,* 447-455, 1973.

Parker, R. L., and S. P. Huestis, The inversion of magnetic anomalies in the presence of topography, *J. Geophys. Res., 79,* 1587-1593, 1974.

Parker, R. L., and D. W. Oldenburg, Thermal model of ocean ridges, *Nature, 242,* 137-139, 1973.

Parsons, B., and J. G. Sclater, An analysis of the variation of ocean floor bathymetry and heat flow with age, *J. Geophys. Res., 82,* 803-827, 1977.

Phillips, J. D., and H. S. Fleming, Multibeam sonar study of the Mid-Atlantic Ridge rift valley, 36°-37°N, *Geol. Soc. Am. Bull., 88,* 1-5, 1977.

Phipps Morgan, J., and D. W. Forsyth, Three-dimensional flow and temperature perturbations due to a transform offset: Effects on oceanic crustal and upper mantle structure, *J. Geophys. Res., 93,* 2955-2966, 1988.

Pockalny, R. A., R. S. Detrick, and P. J. Fox, Morphology and tectonics of the Kane transform from Sea Beam bathymetry data, *J. Geophys. Res., 93,* 3179-3193, 1988.

Pockalny, R. A., P. Gente, and R. Buck, Oceanic transverse ridges: A flexural response to fracture-zone-normal extension, *Geology, 24,* 71-74, 1996.

Purdy, G. M., J.-C. Sempéré, H. Schouten, D. L. Dubois, and R. Goldsmith, Bathymetry of the Mid-Atlantic Ridge, 24° - 31° N: A map series, *Mar. Geophys. Res., 12,* 247-252, 1990.

Rognstad, M., HAWAII MR1: A new underwater mapping tool, paper presented at International Conference on Signal Processing and Technology, DSP Associates, Boston, Mass., 1992.

Rommevaux, C., C. Deplus, P. Patriat, and J. Sempéré, Three-dimensional gravity study of the Mid-Atlantic Ridge: Evolution of the segmentation between 28° and 29°N during the last 10 m.y., *J. Geophys. Res., 99,* 3015-3029, 1994.

Rona, P. A., and D. F. Gray, Structural behavior of fracture zones symmetric and asymmetric about a spreading axis: Mid-Atlantic Ridge (lat. 23°N to 27°N), *Geol. Soc. Am. Bull., 91, Part I,* 485-494, 1980.

Rona, P. A., G. Klinkhammer, T. A. Nelsen, J. H. Trefry, and H. Elderfield, Black smokers, massive sulfides and vent biota at the Mid-Atlantic Ridge, *Nature, 321,* 33-37, 1986.

Schouten, H., and K. D. Klitgord, The memory of the accreting plate boundary and the continuity of fracture zones, *Earth Planet. Sci. Lett.*, *59*, 255-266, 1982.

Schouten, H., and R. S. White, Zero-offset fracture zones, *Geology*, *8*, 175-179, 1980.

Searle, R. C., Multiple, closely spaced transform faults in fast-slipping fracture zones, *Geology*, *11*, 607-610, 1983.

Sempéré, J.-C., G. M. Purdy, and H. Schouten, Segmentation of the Mid-Atlantic Ridge between 24°N and 30°40'N, *Nature*, *344*, 427-431, 1990.

Sempéré, J.-C., P. Blondel, A. Briais, T. Fujiwara, L. Géli, N. Isezaki, J. E. Pariso, L. Parson, P. Patriat, and C. Rommevaux, The Mid-Atlantic Ridge between 29°N and 31°30'N in the last 10 Ma, *Earth Planet. Sci. Lett.*, *130*, 45-55, 1995.

Severinghaus, J. P., and K. C. Macdonald, High inside corners at ridge-transform intersections, *Mar. Geophys. Res.*, *9*, 353-367, 1988.

Shaw, W. J., and J. Lin, Models of ocean ridge lithospheric deformation: Dependence on crustal thickness, spreading rate, and segmentation, *J. Geophys. Res.*, *101*, 17,977-17,993, 1996.

Sloan, H., and P. Patriat, Kinematics of the North American-African plate boundary between 28° and 29°N during the last 10 Ma: Evolution of the axial geometry and spreading rate and direction, *Earth Planet. Sci. Lett.*, *113*, 323-341, 1992.

Smith, D. K., and J. R. Cann, Hundreds of small volcanoes on the median valley floor of the Mid-Atlantic Ridge at 24-30°N, *Nature*, *348*, 152-155, 1990.

Smith, W. H. F., and D. T. Sandwell, Marine gravity field from declassified Geosat and ERS-1 altimetry (abstract), *Eos Trans. AGU*, *76*(46), Fall Meet. Suppl., F156, 1995.

Tolstoy, M., A. J. Harding, and J. A. Orcutt, Crustal thickness on the Mid-Atlantic Ridge: Bull's eye gravity anomalies and focused accretion, *Science*, *262*, 726-729, 1993.

Tucholke, B. E., Massive submarine rockslide on the rift valley wall of the Mid-Atlantic Ridge, *Geology*, *20*, 129-132, 1992.

Tucholke, B. E., and J. Lin, A geological model for the structure of ridge segments in slow-spreading ocean crust, *J. Geophys. Res.*, *99*, 11,937-11,958, 1994.

Tucholke, B. E., and H. Schouten, Kane Fracture Zone, *Mar. Geophys. Res.*, *10*, 1-39, 1988.

Whitehead, J. A., H. J. B. Dick, and H. Schouten, A mechanism for magmatic accretion under spreading centers, *Nature*, *312*, 146-148, 1984.

Yin, A., and J. F. Dunn, Structural and stratigraphic development of the Whipple-Chemehuevi detachment fault system, southeastern California: Implications for the geometrical evolution of domal and basinal low-angle normal faults, *Geol. Soc. Am. Bull.*, *104*, 659-674, 1992.

J. Goff, University of Texas Institute for Geophysics, 8701 N. MoPac Expressway, Austin, TX 78759. (e-mail: goff@utig.ig.utexas.edu)

G. E. Jaroslow, Sea Education Association, P. O. Box 6, Woods Hole, MA 02543. (e-mail: garyj@sea.edu)

M. C. Kleinrock, Department of Geology, Vanderbilt University, Nashville, TN 37235. (e-mail: kleinrmc@ctrvax.vanderbilt.edu)

J. Lin, M. A. Tivey, and B. E. Tucholke, Department of Geology and Geophysics, Woods Hole Oceanographic Institution, Woods Hole, MA 02543. (e-mail: jlin@whoi.edu; moe@deeptow.whoi.edu; btucholke@whoi.edu)

T. B. Reed, Software Development Division, Oceanic Imaging Consultants, 2800 Woodlawn Drive, Suite 150, Honolulu, HI 96822. (e-mail: reed@hammer.oic.htde.org)

(Received July 2, 1996; revised December 6, 1996;
accepted December 11, 1996.)